GLOBAL BIOGEOCHEMICAL CYCLES, VOL. 11, NO. 4, PAGES 507–533, DECEMBER 1997

Carbon 13 exchanges between the atmosphere and biosphere

I. Fung,[1,2] C. B. Field,[3] J. A. Berry,[3] M. V. Thompson,[3,4] J. T. Randerson,[3,4]
C. M. Malmström,[3,4] P. M. Vitousek,[4] G. James Collatz,[5] P. J. Sellers,[6]
D. A. Randall,[7] A. S. Denning,[7] F. Badeck,[8] and J. John[9]

Abstract. We present a detailed investigation of the gross ^{12}C and ^{13}C exchanges between the atmosphere and biosphere and their influence on the $\delta^{13}C$ variations in the atmosphere. The photosynthetic discrimination Δ against ^{13}C is derived from a biophysical model coupled to a general circulation model [*Sellers et al.*, 1996a], where stomatal conductance and carbon assimilation are determined simultaneously with the ambient climate. The $\delta^{13}C$ of the respired carbon is calculated by a biogeochemical model [*Potter et al.*, 1993; *Randerson et al.*, 1996] as the sum of the contributions from compartments with varying ages. The global flux-weighted mean photosynthetic discrimination is 12–16‰, which is lower than previous estimates. Factors that lower the discrimination are reduced stomatal conductance and C_4 photosynthesis. The decreasing atmospheric $\delta^{13}C$ causes an isotopic disequilibrium between the outgoing and incoming fluxes; the disequilibrium is ~0.33‰ for 1988. The disequilibrium is higher than previous estimates because it accounts for the lifetime of trees and for the ages rather than turnover times of the biospheric pools. The atmospheric $\delta^{13}C$ signature resulting from the biospheric fluxes is investigated using a three-dimensional atmospheric tracer model. The isotopic disequilibrium alone produces a hemispheric difference of ~0.02‰ in atmospheric $\delta^{13}C$, comparable to the signal from a hypothetical carbon sink of 0.5 Gt C yr^{-1} into the midlatitude northern hemisphere biosphere. However, the rectifier effect, due to the seasonal covariation of CO_2 fluxes and height of the atmospheric boundary layer, yields a background $\delta^{13}C$ gradient of the opposite sign. These effects nearly cancel thus favoring a stronger net biospheric uptake than without the background CO_2 gradient. Our analysis of the globally averaged carbon budget for the decade of the 1980s indicates that the biospheric uptake of fossil fuel CO_2 is likely to be greater than the oceanic uptake; the relative proportions of the sinks cannot be uniquely determined using ^{12}C and ^{13}C alone. The land-ocean sink partitioning requires, in addition, information about the land use source, isotopic disequilibrium associated with gross oceanic exchanges, as well as the fractions of C_3 and C_4 vegetation involved in the biospheric uptake.

[1]NASA Goddard Institute for Space Studies, New York.

[2]School of Earth and Ocean Sciences, University of Victoria, Victoria, British Columbia, Canada.

[3]Department of Plant Biology, Carnegie Institution of Washington, Stanford, California.

[4]Department of Biological Sciences, Stanford University, Stanford, California.

[5]NASA Goddard Space Flight Center, Greenbelt, Maryland.

[6]NASA Johnson Space Flight Center, Houston, Texas.

[7]Department of Atmospheric Sciences, Colorado State University, Fort Collins.

[8]Laboratoire d'Ecologie Vegetale, Universite de Paris Sud XI, Orsay, France.

[9]Department of Applied Physics, Columbia University, New York.

Copyright 1997 by the American Geophysical Union.

Paper number 97GB01751.
0886-6236/97/97GB-01751$12.00

1. Introduction

Since the beginning of the industrial era, the combustion of fossil fuels has released a total of ~250 Gt (1 Gt = 10^{12} kg) of carbon into the atmosphere. Over the same period, land use modification in the middle latitudes, and more recently in the tropics, has released another ~100 Gt C. The ~150 Gt C increase in CO_2 in the atmosphere, from ~280 parts per million by volume (ppmv) in 1800 to 351 ppmv in 1988, is equivalent to ~60% of the fossil fuel release or ~40% of the total anthropogenic CO_2 source. Balancing the carbon budget requires both the oceans and terrestrial biosphere to have acted as repositories, or sinks, for the anthropogenic CO_2. Direct measurements of CO_2 reservoir sizes and of CO_2 fluxes into and out of the oceans and terrestrial biosphere are sparse, and the methodologies for extrapolating laboratory or site measurements to the globe are under considerable debate. Hence estimates of the global strengths

of the terrestrial and oceanic sinks have not been established with certainty.

CO_2 is nearly but not completely mixed in the atmosphere. The mixing time of CO_2 and other inert trace gases in the atmosphere is about 3 months within a hemisphere and about 1 year between the hemispheres. Therefore information about broad patterns of CO_2 exchanges between the atmosphere and different carbon reservoirs can be extracted from the geographic and temporal variations of carbon dioxide in the atmosphere with the aid of atmospheric transport models [e.g., *Keeling et al.*, 1989a; *Tans et al.*, 1990; *Enting et al.*, 1993, 1995; *Ciais et al.*, 1995a,b]. Over 90% of the fossil fuel emission is from the northern hemisphere, and most of the emission from land use modification is from the tropics. If all the anthropogenic CO_2 remained airborne, this would yield a hemispheric gradient that is larger than that observed (Figure 1). Fossil fuel CO_2 has a $\delta^{13}C$ of -24 to $-28‰$ [*Andres et al.*, 1996], typical of the plant material from which fossil fuels are derived. The anthropogenic emissions, if all airborne, would produce an atmospheric $\delta^{13}C$ gradient that mirrors the CO_2 gradient, with isotopic ratios $0.3‰$ lower in the northern than in the southern hemisphere (Figure 1b). This compares with the observed gradient of $-0.2‰$ [*Keeling et al.*, 1989b; *Ciais et al.*, 1995a; *Trolier et al.*, 1996].

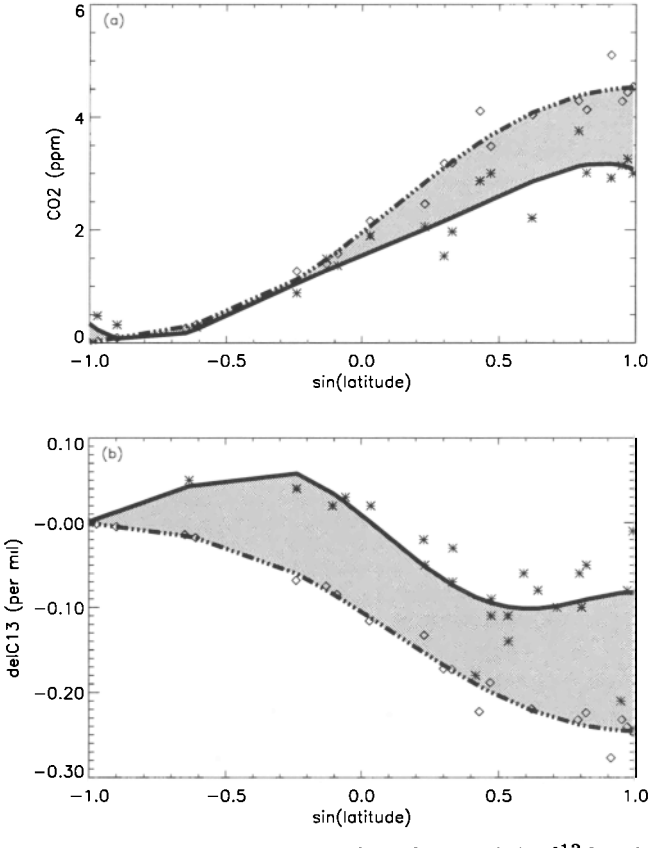

Figure 1. Latitudinal profiles of (a) CO_2 and (b) $\delta^{13}C$, relative to the values at the south pole. The asterisks represent observed values at the National Ocean and Atmospheric Administration (NOAA) monitoring sites. The diamonds are the modeled values at the same sites if all the fossil fuel and land use CO_2 remained airborne. The solid curves are the polynomial curve fits to the observed data, and the dotted-dashed curves are the polynomial curve fits to the modeled fossil fuel and land use contributions. The differences between the modeled and observed curves must be matched by the combined biospheric and oceanic gross and net fluxes.

Retrieving information about carbon sources and sinks from the atmospheric CO_2 gradients requires ancillary data. *Tans et al.* [1990] did not have access to $\delta^{13}C$ information at the time and used a compilation of available marine pCO_2 measurements in their atmospheric tracer transport model calculation. They inferred that midlatitude northern hemisphere land surface may have acted as a significant sink for anthropogenic CO_2. *Keeling et al.* [1989a] used their own $\delta^{13}C$ measurements in their atmospheric tracer model and deduced for the early 1980s an oceanic sink that has approximately the same magnitude as the terrestrial sink. *Ciais et al.* [1995a,b] combined the atmospheric $\delta^{13}C$ data for 1992–1993 with the oceanic pCO_2 and $\delta^{13}C$ measurements in their two-dimensional atmospheric transport model and deduced that the northern middle-to-high-latitude terrestrial biosphere was a sink as large as 3.5 Gt C yr^{-1} for those 2 years. Sinks of this magnitude may, however, be unusual, because these 2 years had significant climatic perturbation. When the atmospheric $\delta^{13}C$ variations are used to constrain the estimates of land-sea partitioning of the anthropogenic CO_2 sink, additional information or assumptions are required to specify fractionation coefficients associated with each CO_2 flux into and out of the atmosphere [*Tans*, 1980; *Fung*, 1993; *Tans et al.*, 1993]. Our relative ignorance about the isotopic fractionation by the gross fluxes remains a major uncertainty in the application of the atmospheric $\delta^{13}C$ variations to the carbon budget.

An appreciation for how accurately one needs to know the isotopic coefficients can be obtained from examining Figure 1. After the signatures of fossil fuel burning and deforestation have been subtracted out, the atmospheric $\delta^{13}C$ north-south gradient to be explained by the combined effects of gross and net biospheric and oceanic exchanges is only $\sim 0.1‰$. A hypothetical sink of 1 Gt C yr^{-1} into the northern middle- or high-latitude terrestrial biosphere would yield, in the tracer model used in this study (described below), an atmospheric CO_2 gradient of 0.5–1.0 ppmv and an atmospheric $\delta^{13}C$ gradient of $\sim 0.05‰$. This sets the "accuracy" criterion for estimating the gradient due to the background biosphere and ocean. The uncertainties in the residual $\delta^{13}C$ profiles (after the effects of gross biospheric and oceanic exchanges have been subtracted from the observed atmospheric gradients) must be less than $0.02‰$ if we are to determine the net biospheric sink to ± 0.5 Gt C yr^{-1}.

In this paper, we present a detailed examination of the factors important for determining the atmospheric ^{13}C signatures associated with gross biospheric exchanges and the

uncertainties contained therein. This is a necessary first step to quantify how much information about the biospheric sink is contained in the atmospheric ^{13}C measurements. We do not carry out a deconvolution of the contemporary carbon budget since we are lacking a parallel examination of gross oceanic exchanges.

We estimate the $\delta^{13}C$ of the CO_2 absorbed and released during photosynthesis and respiration from the results of two biospheric process models. The models are simple biosphere scheme (SiB2) incorporated in the Colorado State University (CSU) general circulation model (GCM) [*Sellers et al.*, 1996a,b; *Randall et al.*, 1996] and the Carnegie-Ames-Stanford Approach (CASA) [*Potter et al.*, 1993; *Randerson et al.*, 1996]. These ^{13}C fluxes are used as inputs to the Goddard Institute for Space Studies (GISS) tracer transport model [*Fung et al.*, 1983, 1987, 1991; *Tans et al.*, 1990] to estimate the sensitivity of the atmospheric $\delta^{13}C$ signatures to different formulations of the gross biospheric ^{13}C exchanges. The implications of our findings on the global carbon budget are discussed. We conclude with suggestions of measurements that may improve our use of $\delta^{13}C$ to characterize and quantify the anthropogenic CO_2 sink.

The commonly used symbols are indicated in the notation list. Fluxes are defined positive into the atmosphere, with F_{ij} denoting fluxes from reservoir i to reservoir j. We use two subscripts, A and a, to denote the atmosphere. The subscript A refers to the total atmospheric signature resulting from all sources and sinks, whereas the subscript a refers to the atmospheric signature resulting from exchanges with a particular reservoir. C_A is the total carbon inventory in the atmosphere, derived from the atmospheric observations. We also use two time variables to separate the important timescales: the long-term variations t and seasonal variations t_s.

2. Observed Atmospheric $\delta^{13}C$ Variations

Since 1991, high-precision measurements of δ_A have been made at the Institute of Arctic and Alpine Research (INSTAAR) on flask samples routinely collected at National Oceanic and Atmospheric Administration Climate Monitoring and Diagnostics Laboratory's (NOAA CMDL) ~44 cooperative network sites and two regular ocean crossings [*Trolier et al.*, 1996]. Prior to that time, δ_A was measured on limited aircraft samples [*Nakazawa et al.*, 1993] and at only a limited number of sites by groups at the Scripps Institution of Oceanography (SIO) and Commonwealth Scientific and Industrial Research Organization (CSIRO) [*Keeling et al.*, 1989b, 1995; *Francey et al.*, 1995]. There are large differences between interannual variations in δ_A in the early portions of the SIO and CSIRO records [*Francey et al.*, 1995]. Here we focus on the long-term trends common to all the available time series and on the seasonal variations found in the NOAA CMDL δ_A data.

Atmospheric δ_A was $-6.4‰$ around 1740 and $-6.8‰$ in 1940 [*Friedli et al.*, 1986; *Leuenberger et al.*, 1992] and decreased rapidly thereafter to $\sim -7.8‰$ in 1988 [*Keeling et al.*, 1989b; *Francey et al.*, 1995]. The decrease is principally the result of the addition of fossil carbon with low isotopic ratios. Since 1988, the decrease in δ_A has slowed most likely as a result of response of the terrestrial biosphere to interannual climate perturbations [*Francey et al.*, 1995; *Keeling et al.*, 1995].

From the NOAA CMDL/INSTAAR observations [*Trolier et al.*, 1996], $\delta_A(x, y, t_s, t)$ varies by $0.2‰$ between the northern and southern hemispheres for the period 1992–1993. The seasonal peak-trough amplitude is $0.89‰$ at Point Barrow, Alaska (71°N), and $0.36‰$ at Mauna Loa, Hawaii (19°N). The phasing of the $\delta^{13}C$ cycles is opposite to that of the CO_2 cycles, with the lowest $\delta^{13}C$ values occurring at the beginning of the growing season and the highest occurring at the end of the growing season.

3. The Modeling Framework

In this study we focus on the atmospheric CO_2 and $\delta^{13}C$ signatures of the exchanges with the terrestrial biosphere and use the following equations as a framework for our analysis:

$$\frac{\partial}{\partial t}(C_a) + \mathcal{T}(C_a) = F_{ap} + F_{ba} \tag{1a}$$

$$C_A \frac{\partial}{\partial t}(\delta_a) + C_A \mathcal{T}(\delta_a) = -\Delta \times F_{ap} + (\delta_b - \delta_A) \times F_{ba} \tag{1b}$$

In equations (1a) and (1b), $\mathcal{T}$ is the atmospheric transport operator, which has zero contribution when integrated over the entire global atmosphere. The subscript p denotes the photosynthetic product, while b denotes the detrital and soil pools. We use F_{ap} rather than F_{ab} to denote the photosynthetic flux to emphasize that different carbon pools and different fractionation processes are involved in photosynthesis and respiration.

The δ_A on the right hand side of equation (1b) is the atmospheric $\delta^{13}C$ during photosynthesis. The $\delta^{13}C$ averaged over the growing season is close to the annual mean. We therefore approximate δ_A in equation (1b) by its hemispherically averaged annual-mean value.

In this study we assume that autotrophic respiration is proportional to the instantaneous gross primary production (GPP), with the proportionality constant spatially and temporally invariant. We further assume that CO_2 respired by autotrophs is of recent origin and carries the isotopic signature of the recently formed plant material. In this way, F_{ap} in equations (1a) and (1b) is given by the net primary production (NPP), the difference between GPP and autotrophic respiration, and F_{ba} is the CO_2 release due to heterotrophic respiration. While these assumptions about autotrophic respiration are mathematically convenient and commonly employed in studies of the global carbon cycle [e.g., *Heimann and Keeling*, 1989], there is little theory or data to support or contradict them.

To focus on the perturbation in the exchanges in the recent decades, we first assume an equilibrium in the preindustrial era with a balance in both gross ^{12}C and ^{13}C fluxes into and out of the biosphere. Let q be any variable. The symbol $\widetilde{q}$ will denote flux-weighted averaging over seasonal variations in q, while $\overline{q}$ will denote the long-term flux-weighted average of q.

In the preindustrial equilibrium, it follows from equations (1a) and (1b) that at each location (x, y)

$$\int_y \int_{mos} F_{ap}(t_s,t)dt_s dt = -\int_y \int_{mos} F_{ba}(t_s,t)dt_s dt \quad (2)$$

$$\begin{aligned}\overline{\widetilde{\delta_b}} &= \frac{\int_y \int_{mos} F_{ba}(t_s,t)\delta_b(t_s,t)dt_s dt}{\int_y \int_{mos} F_{ba}(t_s,t)dt_s dt} \\ &= \frac{\int_y \int_{mos} F_{ap}(t_s,t)[\delta_A(t_s,t) - \Delta(t_s,t)]dt_s dt}{\int_y \int_{mos} F_{ap}(t_s,t)dt_s dt} \\ &= \overline{\widetilde{\delta_A}} - \overline{\widetilde{\Delta}} = \overline{\widetilde{\delta_p}}. \end{aligned} \quad (3)$$

There are two noteworthy points about equations (2) and (3). Even with an equilibrium, F_{ap} and F_{ba} do not balance every month, and it is not meaningful to rewrite equations (1a) and (1b) in terms of gross and net fluxes when seasonal effects are considered. The flux-weighted mean $\delta^{13}C$ of the plant material equals the flux - weighted mean δ_b of the respired carbon, which is not the same as the mass - weighted mean δ_b obtained from soil samples. As has been pointed out by *Lloyd et al.* [1996], care must therefore be exercised in applying soil $\delta^{13}C$ measurements to the atmospheric problem.

In the era with anthropogenic CO_2 emissions, a ^{12}C flux equilibrium between the atmosphere and biosphere may no longer exist because of net uptake of CO_2 by the biosphere. Even if equation (2) holds, the gross ^{13}C fluxes would no longer balance, since the atmospheric δ_A and hence δ_b are changing with time. Photosynthesis removes "light" carbon

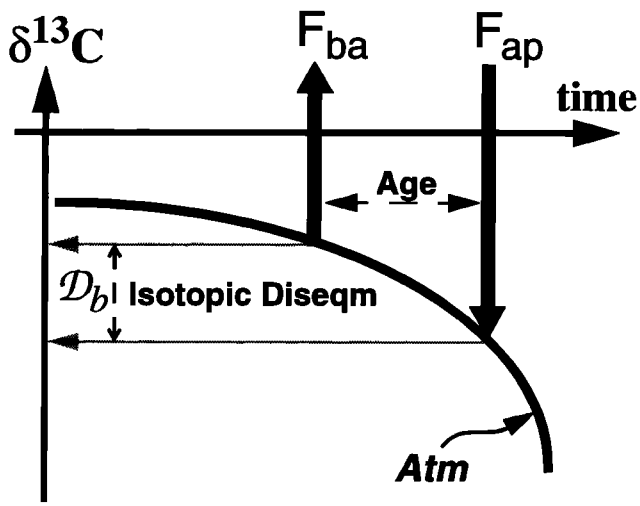

Figure 2. Schematic diagram of isotopic disequilibrium.

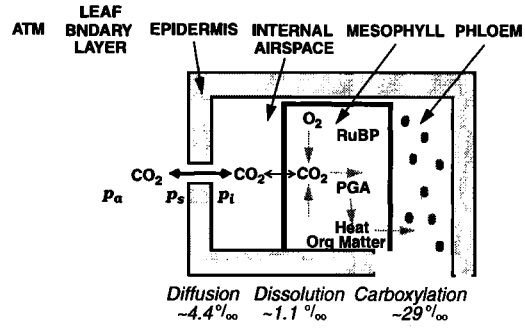

Figure 3. Schematic diagram of the ^{13}C fractionation steps involved during photosynthesis and typical values of the discrimination associated with each step. Discrimination is expressed in per mil.

with the modern δ_A value, whereas respiration delivers "old" carbon, whose $\delta^{13}C$ value depends on how long the carbon has been away from the atmosphere. There is thus an isotopic disequilibrium between incoming and outgoing fluxes [*Fung*, 1993; *Tans et al.*, 1993; *Ciais et al.*, 1995a,b; *Francey et al.*, 1995]. This is illustrated schematically in Figure 2. In the following sections, we describe the modeling of Δ and isotopic disequilibrium and evaluate their consequences on the atmospheric $\delta^{13}C$.

4. Photosynthesis

CO_2 from the atmosphere is processed in several steps before it is incorporated into plant material (Figure 3). Briefly, the steps include gaseous diffusion across the laminar boundary layer to the surface of the leaf and across the stomatal opening into the intercellular air spaces of the leaf. CO_2 then dissolves in the aqueous phase and diffuses across the cell wall and cellular membranes to the chloroplasts. In the chloroplasts, CO_2 is chemically combined with an acceptor molecule in an enzyme catalyzed carboxylation reaction. Different carboxylation reactions occur in C_3 and C_4 species. Fractionation against $^{13}CO_2$ occurs in all steps that transfer CO_2 from the atmosphere to the chloroplast and in the carboxylation reactions. These discrimination factors are known from experiments with model systems (for reviews see *O'Leary* [1981, 1989] and *Farquhar et al.* [1989]). The net discrimination associated with the sequence of steps that occurs in photosynthesis, Δ, is a "weighted sum" of the discrimination associated with the individual steps in the sequence. For example, *Farquhar et al.* [1982] showed that two steps, gaseous diffusion and carboxylation, combined as

$$\Delta = a + (b - a)p_i/p_a \quad (4)$$

where p_i and p_a are the partial pressures of CO_2 in the intercellular air spaces of the leaf and in the ambient atmosphere, respectively, a is the intrinsic discrimination in gaseous diffusion (4.4‰), and b is that associated with the biochemical fixation of CO_2 (27.5 and 3 to 6‰ for C_3 and C_4 plants, re-

spectively). This equation has been widely used to interpret carbon isotope discrimination in photosynthesis. However, it should be noted that this is an approximation since several steps (diffusion in the boundary layer, dissolution of CO_2 in water, and diffusion in the aqueous phase) are ignored in equation (4). A more complete equation is given by *Evans et al.* [1986], but equation (4) captures the primary effects.

We may gain a better feel for the behavior of equation (4) by noting that $\Delta = a$ when $p_i/p_a = 0$ and $\Delta = b$ when $p_i/p_a = 1$ and that the values of a and b are similar for C_4 plants and very different for C_3 plants. Thus Δ of C_3 plants is variable ($4.4 \leq \Delta \leq 27.5$), while that for C_4 plants is relatively constant ($3 \leq \Delta \leq 5$). It is also important that p_i is expected to vary with time so that (at least for C_3 plants) we must integrate the instantaneous values of Δ and the net CO_2 assimilation (A_n) through time to get the isotopic composition of the accumulated products of photosynthesis.

Integration of discrimination through time and for the whole globe is a complex problem since both A_n and p_i/p_a may vary on a time scale of minutes. *Lloyd and Farquhar* [1994] approached this problem by estimating mean monthly values of p_i/p_a and NPP from global maps of vegetation cover, elevation, temperature, precipitation, and atmospheric humidity. To do this, they make some adjustments to the climatic variables to approximate the microclimate of a leaf during photosynthesis, and they assume that weighted average discrimination over a month is the same as discrimination under an environmental condition they select as representative of that month. The global maps of annual integrated discrimination produced by *Lloyd and Farquhar* [1994] are plausible, and their predicted discrimination predicts the $\delta^{13}C$ of plant biomass in several calibration sites reasonably well. However, their approach has limited scope for studies of the annual cycle and interannual variation. In this study, we have opted to take an alternative approach that permits calculation of A_n and Δ in an atmospheric general circulation model. This has lower spatial resolution than the approach taken by Lloyd and Farquhar, but since photosynthesis and p_i/p_a are calculated at each time step (0.1 hour) of the model, the time resolution is appropriate to capture most of the variation in Δ.

The approach we use to model photosynthesis in this study follows from the work of *Farquhar et al.* [1980], who express the CO_2 assimilation rate A_n as proportional to the CO_2 partial pressure gradient across the stomata:

$$A_n = \frac{g_s}{1.6}\frac{p_s - p_i}{p_s} = \frac{g_b}{1.4}\frac{p_a - p_s}{p_a} \tag{5}$$

where g_s is the stomatal conductance, g_b is the leaf boundary layer conductance, p_i, p_s, and p_a are the intercellular, leaf surface, and ambient CO_2 partial pressures, respectively.

Collatz et al. [1991] extended the work of *Farquhar et al.* [1980] and *Ball et al.* [1987] to develop an empirical model that captures the response of stomatal conductance g_s to environmental and physiological factors:

$$g_s = m\frac{A_n h_s P}{p_s} + g_{s0} \tag{6}$$

where h_s is the relative humidity at the leaf surface, P is the total atmospheric pressure, and m and g_{s0} are empirically determined parameters. The photosynthetic assimilation rate A_n is also limited by the availability of sunlight, substrate, and other abiotic conditions. The *Collatz et al.* [1991, 1992] models are imbedded in SiB2 within the CSU GCM [*Sellers et al.*, 1996a,b; *Randall et al.*, 1996], wherein A_n and g_s are determined simultaneously with the constraint that A_n is the "smoothed" minimum of the light-limited, rubisco/CO_2-limited, and sink-limited (pep carboxylase limited in the case of C_4) assimilation rates [*Collatz et al.*, 1991, 1992]; and there is maximized water use efficiency for instantaneous atmospheric conditions. The vegetation and atmosphere are fully interactive in the CSU GCM, and p_i, p_s, and p_a are calculated at every time step of the GCM integration.

The 6 min values of p_i/p_a, as calculated by SiB2 in the CSU GCM, are weighted by the instantaneous A_n to yield the flux-weighted monthly p_i/p_a, from which the monthly mean Δ is derived, using equation (4).

If all vegetation were C_3 plants, no additional information about vegetation distributions would be required. Obtaining the geographic distribution of Δ requires the distribution of C_4 plants. The vegetation distribution used in the CSU GCM is derived from ground-based observations [*Dorman and Sellers*, 1989; *Sellers et al.*, 1996a]. As such, it does not distinguish between C_3 and C_4 vegetation. We assume mixtures of C_3-C_4 plants in the ratios of 25:75 for savannas and of 50:50 for shrubs with ground cover. Cultivation is assumed to be comprised of C_3 vegetation. We consider this distribution to be representative of the current vegetation.

The annual mean flux-weighted $\Delta(x, y)$ distribution (not shown) modeled as above is similar to that presented by *Lloyd and Farquhar* [1994]. The major geographic variations are due to discrimination by C_3 ($\Delta \sim 18‰$) versus C_4 plants ($\Delta = 4.4‰$) [e.g., *Lloyd and Farquhar*, 1994]. Among C_3 plants, $\overline{\Delta}$ ranges between 15 and 24‰, reflecting variations in climate and in biophysics captured in SiB2-GCM. The systematics of Δ variations compares with the measurements of *Körner et al.* [1991] which show a comparable pattern albeit smaller range, $\sim 3.5‰$, in leaves of lowland plants not limited by water or sunlight.

The flux- and area-weighted annual-mean $\overline{\Delta}$ is 15.7‰ for the current vegetation distribution, with mixtures of C_3 and C_4 plants in savanna and shrubs. If these vegetation types consisted only of C_4 plants, the value would be 14.7‰ If there were no C_4 vegetation, $\overline{\Delta}$ would be 20.0‰.

Our Δ value of 20.0‰ for C_3 vegetation is higher than the value of 17.8‰ reported by *Lloyd and Farquhar* [1994]. In both studies, the latitudinal variations in the annual mean Δ of C_3 plants are small (Figure 4). At high latitudes, the $\overline{\Delta}$ simulated by SiB2-GCM is higher by as much as ~4–

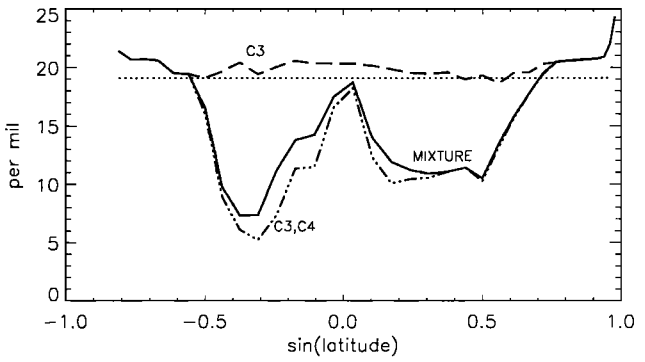

Figure 4. Latitudinal distribution of the zonal-mean flux-weighted photosynthetic discrimination Δ, as modeled by the simple biosphere scheme general circulation model (SiB2-GCM) for the current vegetation with C_3:C_4 mixtures in savannas and shrublands (see text, solid curve), for current vegetation without mixtures (dotted-dashed curve), and for C_3 vegetation only (dashed curve). The dotted curve (Δ=18.6) is that in equilibrium with δ_A = -6.4 ‰ and δ_b = -25 ‰.

5‰. While our results for the boreal forests (~19–20‰) are more consistent with the 19.1‰ estimated from measurements made during the Boreal Ecosystem-Atmosphere Study (BOREAS) campaigns [*Flanagan et al.*, 1996] compared to the corresponding *Lloyd and Farquhar* [1994] value of ~14–16‰, we have neglected fractionation that occurs during diffusion between the interior of the stomata and the sites of carboxylation while *Lloyd and Farquhar* [1994] treat this explicitly. This difference would produce a ~3‰ difference for C_3 plants between the two studies. The difference would be smaller at low latitudes. The fractionation due to this additional diffusion step is likely to account for the difference between the two studies. The neglect of this diffusional fractionation is not likely to affect our inferences about the atmospheric $\delta^{13}C$ signature of atmosphere-biosphere exchange, since this fractionation is not likely to alter the seasonality of Δ and will be canceled out when we consider net fluxes in the annual mean.

With the inclusion of C_3:C_4 combinations, our flux-weighted annual mean $\overline{\overline{\Delta}}$ is 4.3‰ lower than our value for C_3 plants only. This C_4 contribution is comparable with the 3‰ found by *Lloyd and Farquhar* [1994]. The difference between the two studies is most likely due to differing areal extents of C_4 vegetation. The small difference in Δ values for C_4 plants, 4.4‰ in our study and ~3.6‰ given by *Lloyd and Farquhar* [1994], tends to increase the impact of C_4 photosynthesis on $\overline{\overline{\Delta}}$ in the work of *Lloyd and Farquhar* [1994], opposite to the difference in the overall results.

SiB2-GCM obtains a globally averaged flux-weighted Δ of 15.7‰. If we include fractionation during diffusion to the carboxylation sites and adopt the *Lloyd and Farquhar* [1994] value for C_4 Δ and a larger areal extent of C_4 vegetation, we would obtain a $\overline{\overline{\Delta}}$ that is ~2–3‰ lower or ~12–13‰. This value is the lowest reported, compared to 14.8 of *Lloyd and Farquhar* [1994], 17.6 of *Keeling et al.* [1989b], 20.0 of *Quay et al.* [1992], and 18.0 of *Tans et al.* [1993]. *Lloyd and Farquhar* [1994] point out the neglect of C_4 plants in the other studies yields an unrealistically high discrimination and would have an impact on the carbon source/sink analysis. The implication for the global carbon budget is explored later in this study.

On the basis of the increase of Δ with A_n and g_s, one might expect that Δ would be maximum at the height of the growing season, generally in the summer, when relative humidity is high. However, Δ decreases with the ratio A_n/g_s (compare equations (4), (5), and (6)). Indeed, *Lloyd et al.* [1996] found comparable Δ values for Siberia in July and the Amazon forest in September, despite the differences in A_n and g_s. A similar result is found here. The value Δ is 20.5‰ for the tropical rainforest in September and is 21.5‰ for Siberian forests in July. Thus it is not straightforward to predict the phasing of the seasonal cycle of Δ at different locations.

The geographic distribution of the peak-trough range in Δ (Plate 1a) reflects the seasonality of carbon assimilation rates and humidity. For C_3 plants, the seasonal excursions of Δ are largest, >15‰, in high latitude ecosystems and decrease equatorward to ~1.8‰ in tropical rainforests. The latitudinal variations in Δ are shown in Plate 1b. The timing of Δ at several typical sites is shown in Figure 5. At the boreal forest site (105°W, 53°N), the seasonal variations in Δ mirrors the seasonal variations in photosynthesis, and Δ increases from 12.8‰ in March to 20.5‰ in July. The same pattern of a summer maximum Δ is found at the deciduous forest site (100°E, 70°N). At the tundra site (100°W, 62°N), the maximum Δ of 20.8‰ is found in October at the end of the short growing season. By contrast, at the middle-latitude C_3 grassland site (95°W, 46°N), Δ decreases from a value of 19.0‰ in February to a minimum of 14.3‰ in April. These variations reflect the differing rates of increase of A_n and g_s into the growing season. At high latitudes, the low Δ values at the beginning of the growing season (Figure 5), while theoretically possible because of the low relative humidities at low temperatures, may be an artifact of inaccuracies in the GCM simulation. They have not been confirmed or contradicted because of the lack of direct measurements of Δ at that time of year. In any case, they are not likely to affect our inferences about the biospheric signature in atmospheric $\delta^{13}C$: in equation (1b), Δ is multiplied by F_{ap}, which is small in early spring.

5. Respiration

With photosynthesis, the stomata are the sole entry points for atmospheric CO_2. With respiration, CO_2 is released from all components of the ecosystem. To model respiration, it is often convenient to divide the biosphere into compartments (e.g., leaves, roots, trunk, and soil organic matter), each characterized by its function, chemical composition, lifetime, or

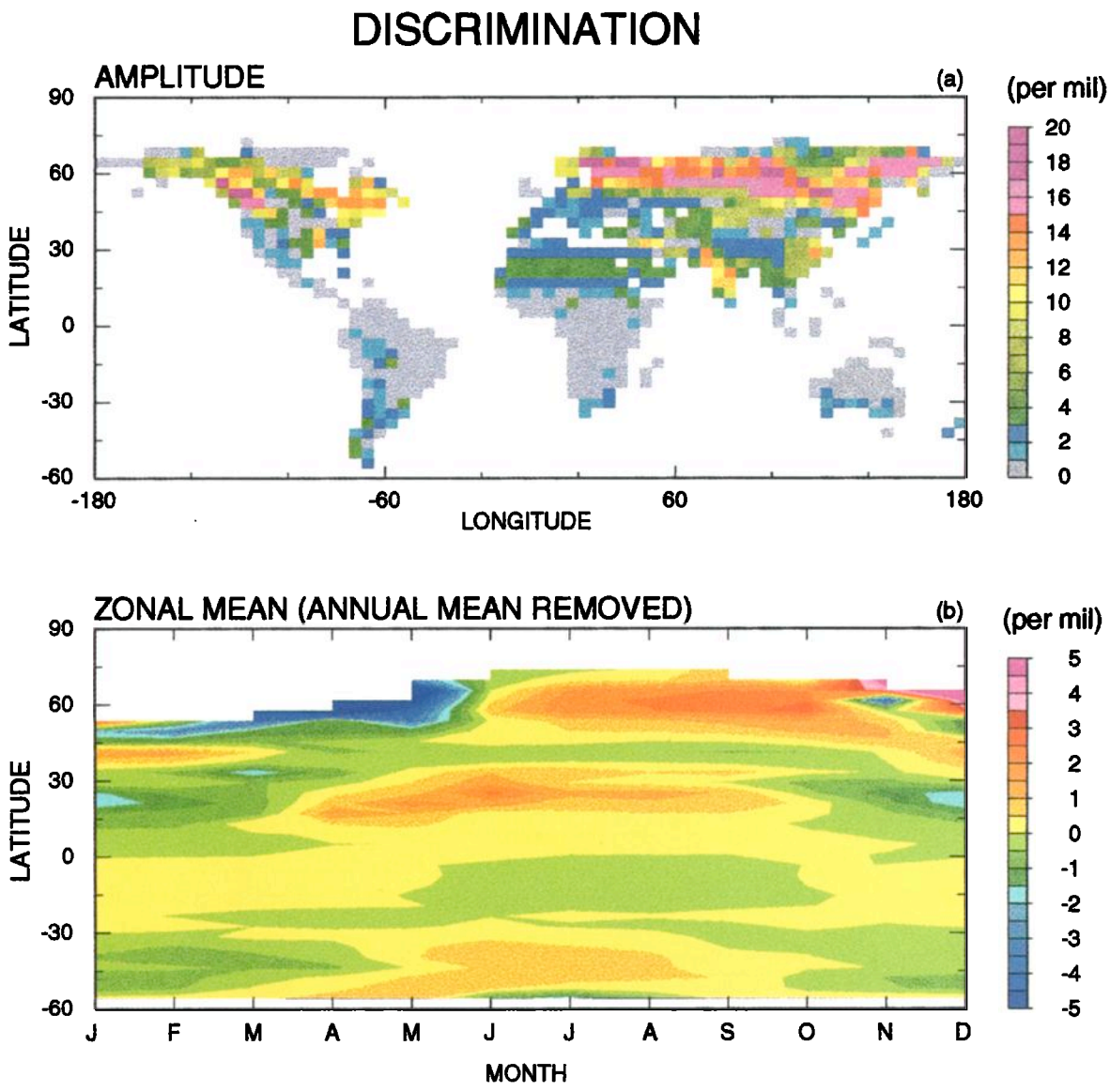

Plate 1. Seasonality in discrimination as modeled by SiB2-GCM: (a) global distribution of the seasonal range and (b) monthly departures from the zonal mean.

other features. The newly assimilated carbon is allocated amongst the live compartments of the plant. Mortality transfers the carbon from the live compartments to the dead compartments. Heterotrophic activity processes the dead plant matter, releasing some of the carbon as CO_2 and transferring some to soil organic matter. CO_2 release thus occurs across all the live and dead compartments. The residence time of carbon in a plant or soil fraction varies from a few days for microbial biomass to centuries for soil organic matter that is physically protected by clay aggregates.

We use the CASA biospheric model [*Potter et al.*, 1993] with updates described by *Randerson et al.* [1996] for investigating the CO_2 and ^{13}C fluxes due to heterotrophic respiration (Figure 6). CASA includes nine litter and soil carbon compartments. The pools are dead metabolic biomass, structural biomass and live microbial biomass at the surface (leaf litter) and in the soil (root litter), as well as woody litter and slow and armored (passive) soil carbon (Tables 1a and b) The transfer of carbon from one pool to another and the CO_2 respired during the transfer are modulated by factors such as temperature, precipitation, lignin content, soil texture, and the carbon assimilation efficiencies of microbes.

Let $f_k(x, y, t_s)$ denote the fraction of the total respired carbon emerging from pool k at the location (x, y) for the month t_s:

$$f_k(x, y, t_s) = \frac{F_{ka}(x, y, t_s)}{\sum_{k=1}^{9} F_{ka}(x, y, t_s)} \tag{7}$$

$$\sum_{k=1}^{9} F_{ka}(x, y, t_s) = F_{ba}(x, y, t_s) \tag{8}$$

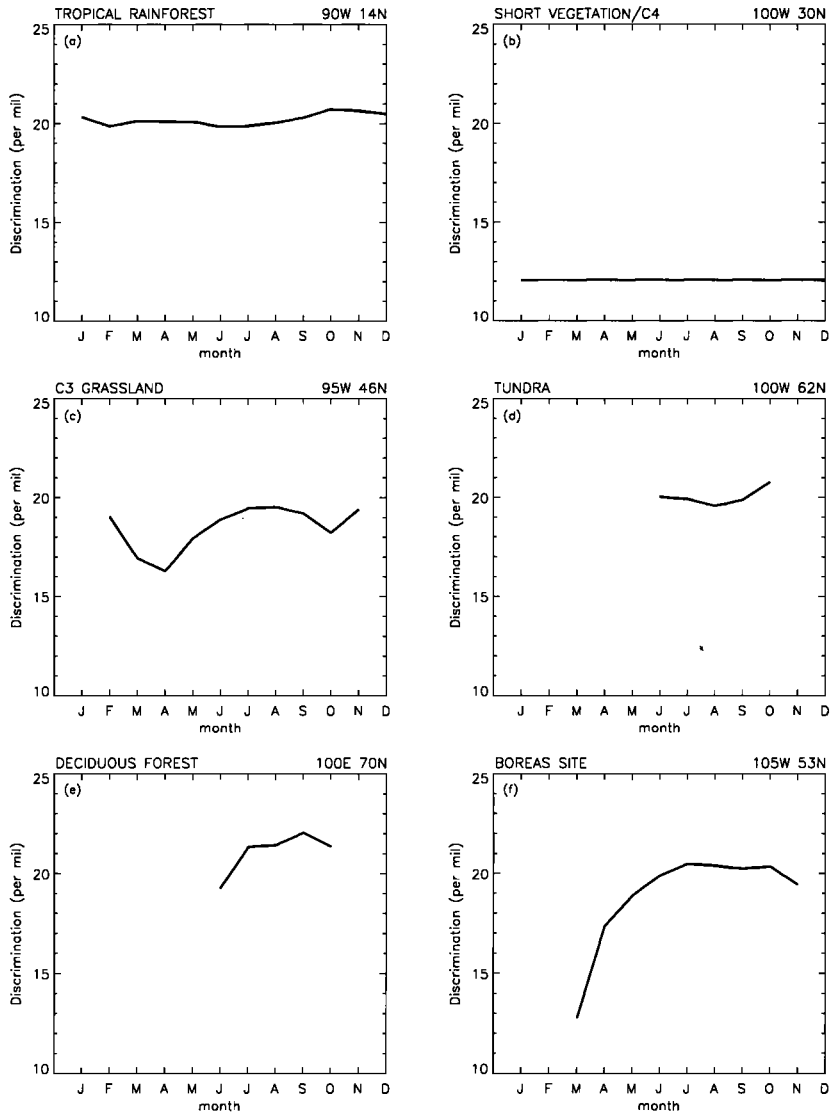

Figure 5. Seasonal variations of the flux-weighted monthly mean discrimination at (a) tropical rainforest (90°W, 14°N), (b) short vegetation, C_4 grassland (100°W, 30°N), (c) C_3 grassland (95°W, 46°N), (d) tundra (100°W, 62°N), (e) deciduous forest (100°E, 70°N), and (f) boreas field site (105°W, 53°N).

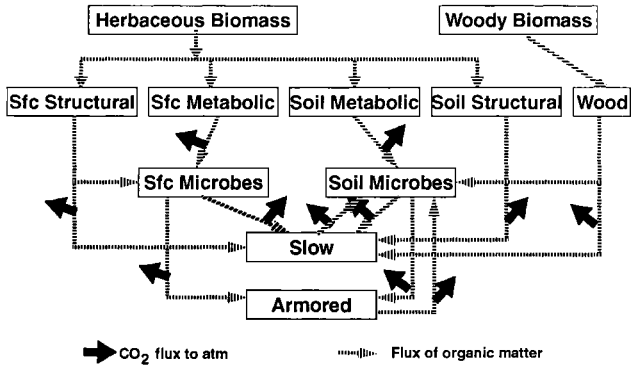

Figure 6. Schematic diagram of the Carnegie-Ames-Stanford approach (CASA) (adapted from *Potter et al.* [1993]).

Equation (8) merely states that the sum of the fluxes from the different pools is the total respiration flux in equation (1b). The annually averaged $f_k(x, y)$ are shown in Table 1a for the different pools of the different ecosystems, while the seasonally varying $f_k(x, y, t_s)$ are shown in Figure 7 for several locations. For the tropical forest, the "slow" pool dominates and accounts for ~ 30% of the total respired flux through the year. The total flux comprises ~8 and 15% from the surface and soil microbial pools, respectively; 10% each from the surface and soil metabolic pools; and 6.6 and 6.3% from the surface and soil structural pools, respectively. The remainder of the fluxes are mainly from the woody litter pool (13%) and the passive pool (0.25%). Even though the seasonal variations of the respiratory flux of CO_2 from tropical forests are small, there is a larger fraction of CO_2 from the

Table 1a. Percentage of Fluxes From Each Biospheric Pool, the Turnover Times of Each Pool, and Ages of Respired Carbon From Each Pool, as Determined by CASA

	Broad-Leaved Evergreen Forest			Broad-Leaved Deciduous Forest			Broad-Leaved and Needle-Leaved Forest		
Pool	Flux, %	TOT	Age	Flux, %	TOT	Age	Flux, %	TOT	Age
srfmet	10.3	0.2	2.0	3.6	0.3	1.6	3.3	0.4	1.8
soilmet	9.4	0.2	2.0	3.4	0.3	1.6	3.1	0.3	1.8
srfstr	6.6	3.4	5.2	14.1	2.6	3.9	14.3	2.8	4.2
soilstr	6.3	2.9	4.7	13.2	2.2	3.5	13.4	2.4	3.8
srfmic	8.1	0.4	14.8	7.9	0.7	19.2	7.9	0.7	21.8
soilmic	14.8	0.7	28.7	15.4	1.1	41.5	16.2	1.1	44.4
wood	13.1	3.7	41.7	12.9	6.4	54.3	12.9	7.0	62.0
slow	31.2	9.1	34.7	29.3	15.9	49.9	28.6	17.3	54.7
arm	0.3	400.7	429.5	0.3	701.9	743.2	0.3	760.5	804.7
All	100.0	5.1	24.1	100.0	8.4	32.7	100.0	8.7	35.8
	Needle-Leaved Evergreen Forest			Needle-Leaved Deciduous Forest			Broad-Leaved Forest With Ground Cover		
Pool	Flux, %	TOT	Age	Flux, %	TOT	Age	Flux, %	TOT	Age
srfmet	3.0	0.4	5.7	3.1	0.5	2.5	10.7	0.2	1.9
soilmet	2.8	0.4	5.6	2.9	0.4	2.5	9.8	0.2	1.9
srfstr	14.6	3.1	8.4	14.6	3.9	5.8	6.9	2.4	4.1
soilstr	13.7	2.6	7.9	13.7	3.3	5.2	6.5	2.0	3.7
srfmic	7.9	0.8	19.8	7.9	1.0	18.3	8.6	0.4	8.3
soilmic	17.3	1.2	43.7	16.8	1.5	48.5	16.4	0.6	21.4
wood	12.9	8.0	45.2	12.9	9.8	45.8	13.1	3.9	21.6
slow	27.5	19.7	52.1	28.0	24.3	57.8	27.8	9.7	26.2
arm	0.2	868.9	911.3	0.2	1072.4	1111.8	0.3	426.3	447.7
All	100.0	9.4	33.8	100.0	11.8	35.8	100.0	4.8	16.4
	Perennial Grassland			Broad-Leaved Shrub With Grass			Broad-Leaved Shrub With Bare Soil		
Pool	Flux, %	TOT	Age	Flux, %	TOT	Age	Flux, %	TOT	Age
srfmet	19.2	0.3	1.9	8.5	0.3	1.7	9.1	0.2	1.9
soilmet	17.7	0.2	1.8	7.9	0.2	1.7	8.4	0.2	1.8
srfstr	9.6	2.5	4.1	12.0	3.4	4.8	8.3	3.2	4.8
soilstr	7.7	2.1	3.7	7.4	2.9	4.3	7.6	2.7	4.3
srfmic	9.9	0.5	2.9	7.7	0.5	7.4	7.9	0.5	6.6
soilmic	17.1	0.8	14.6	15.8	0.8	23.3	17.1	0.7	21.1
wood	0.0	0.0	0.0	12.5	4.8	16.4	12.9	4.5	13.7
slow	18.5	12.5	21.5	28.1	11.8	26.7	28.4	11.2	24.3
arm	0.2	549.8	562.1	0.3	519.0	540.6	0.2	493.8	514.8
All	100.0	4.2	9.4	100.0	6.1	16.4	100.0	5.6	15.1
	Tundra			Bare Soil and Desert			Cultivation		
Pool	Flux, %	TOT	Age	Flux, %	TOT	Age	Flux, %	TOT	Age
srfmet	20.3	0.5	3.1	12.5	0.3	2.0	23.8	0.2	2.0
soilmet	18.8	0.4	3.1	11.5	0.3	1.9	22.0	0.2	2.0
srfstr	9.0	4.6	7.1	7.9	2.7	4.4	5.2	2.0	3.6
soilstr	7.6	3.8	6.4	5.1	2.3	3.9	4.9	1.6	3.3
srfmic	9.8	0.9	5.0	8.9	0.6	5.8	10.8	0.5	2.7
soilmic	17.7	1.3	24.1	18.5	0.7	20.0	15.1	0.7	10.7
wood	0.0	0.0	0.0	12.7	5.3	13.1	0.0	0.0	0.0
slow	16.7	22.3	36.9	22.5	13.2	26.1	17.9	7.9	15.6
arm	0.2	983.7	999.6	0.2	579.6	593.3	0.3	346.0	356.6
All	100.0	6.8	15.2	100.0	5.2	13.8	100.0	2.8	6.9

Turnover times (TOT) and ages are in years.

The nine biospheric pools in CASA are the surface and soil metabolic pools (srfmet, soilmet), surface and soil structural pools (srfstr, soilstr), surface and soil microbial pools (srfmic, soilmic), the woody (wood), slow and armored (arm) pools.

Table 1b. Flux-Weighted $\bar{\tilde{\Delta}}$ and $\bar{\tilde{\mathcal{D}}}_b$ (1988) for the Ecosystems

Ecosystem	$\bar{\tilde{\Delta}}$	$\bar{\tilde{\mathcal{D}}}_b$ (1988)
Broad-leaved evergreen forest	20.1	0.44
Broad-leaved deciduous forest	19.6	0.49
Broad-leaved and needle-leaved forest	20.1	0.49
Needle-leaved evergreen forest	20.5	0.54
Needle-leaved deciduous forest	20.1	0.51
Broad-leaved forest with ground cover	12.1	0.38
Perennial grassland	4.4	0.20
Broad-leaved shrub with grass	8.2	0.25
Broad-leaved shrub with bare soil	19.1	0.28
Tundra	18.6	0.32
Bare soil and desert	4.3	0.21
Cultivation	20.0	0.18

In per mil.

slow, microbial, and structural compartments in the summer than in the winter. With seasonal vegetation, such as deciduous or boreal forests, not only is the respired CO_2 flux highly seasonal, the "composition" of the flux is varying through the year. The seasonal variation of flux fraction from these pools can be as large as ~20%.

The impact of the respiratory flux on atmospheric $\delta^{13}C$ is represented by $F_{ba} \times (\delta_b - \delta_A)$, the second term on the right-hand side of equation (1b). With equation (7), we can write

$$F_{ba}(x,y,t_s)\delta_b(x,y,t_s,t) = \sum_k F_{ka}(x,y,t_s)\delta_{b,k}(x,y,t_s,t) \tag{9}$$

or

$$\delta_b(x,y,t_s,t) = \sum_k f_k(x,y,t_s)\delta_{b,k}(x,y,t_s,t) \tag{10}$$

Equation (10) states that the mean $\delta_b(x,y,t_s,t)$ that needs to be determined is the flux-weighted mean δ_b of all the pools. A direct method for estimating the δ_b of the respired CO_2 is by an empirical relationship between nighttime $\delta^{13}C$ and CO_2 concentrations [*Keeling*, 1958, 1961; *Lloyd et al*, 1996]. This avoids integration over the different carbon pools but yields little insight into the dynamics of $\delta^{13}C$ of respiration.

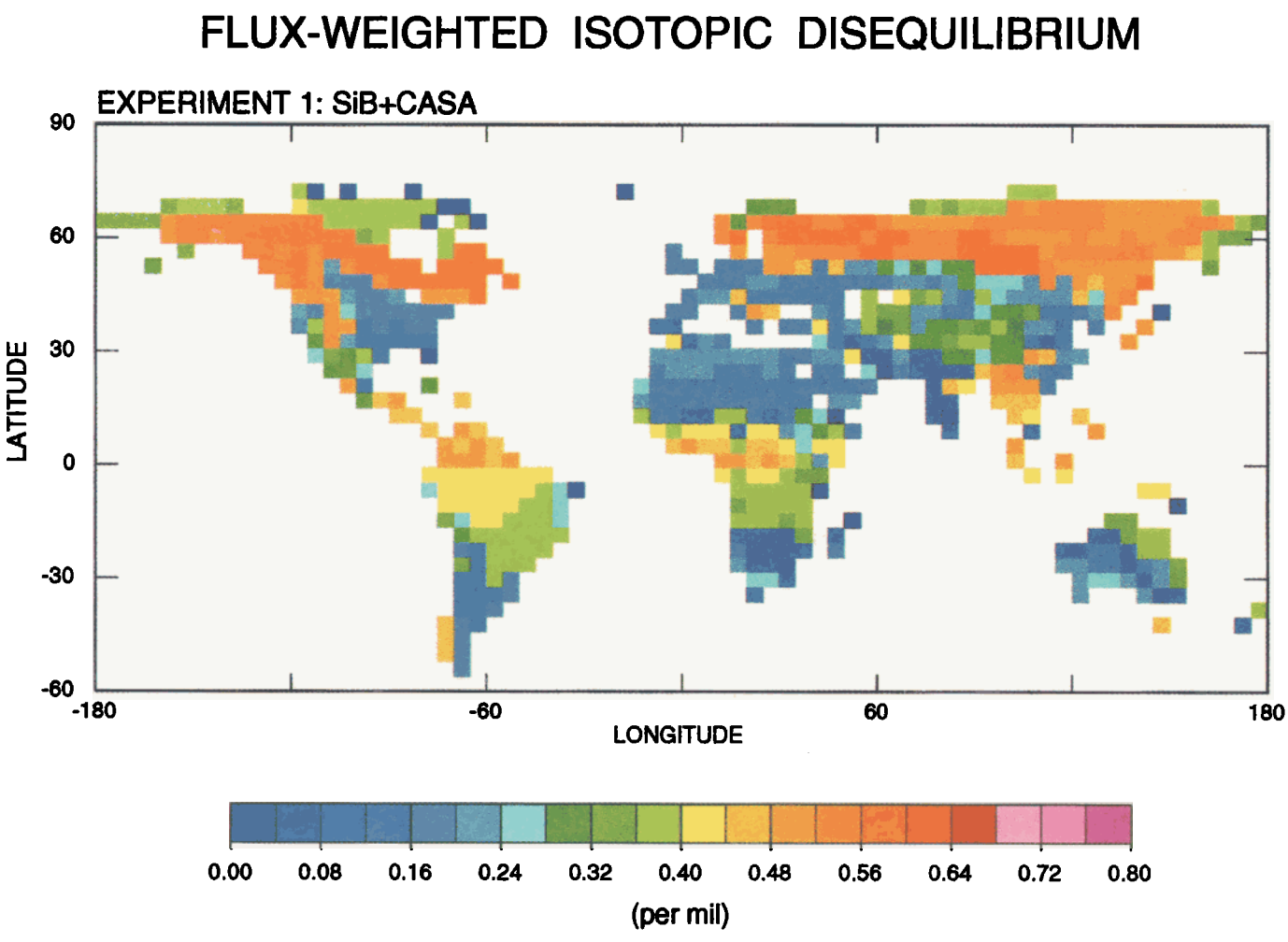

Plate 2. Global distribution of the annual-mean flux-weighted isotopic disequilibrium, averaged for the 1980s, between gross exchange of CO_2 between the atmosphere and biosphere

Measurements of $\delta_{b,k}$ show significant variations among the different plant components. For example, roots have been measured to be isotopically heavier than leaves and stems [*Lauteri et al.*, 1993] by $\sim 0.5‰$. Also, with tall vegetation, the variations of light intensity, temperature, humidity, and CO_2 concentration within the canopy give rise to different assimilation rates and carbon discrimination at different heights in the canopy [e.g., *Francey and Farquhar*, 1982; *Broadmeadow and Griffiths*, 1993]. The value δ_p may vary by as much as $6.5‰$ across 30 m in the canopy, with the isotopically lighter material near the surface where the assimilated CO_2 comprises a larger fraction of respired CO_2 than at the top of the canopy [*Broadmeadow and Griffiths*, 1993]. These variations are larger than the $0.02‰$ criterion sought in this study.

These local scale variations, though invaluable for understanding the dynamics of assimilation, allocation, and respiration, turn out to be unimportant for unraveling the changing signature of biospheric exchanges on atmospheric ^{13}C, as long as the relative flux contributions, $f_k(x, y, t_s)$, are known and are not changing with time. This is because in a multiyear steady state, the total respired isotopic flux from all compartments must balance the incoming flux. A flux from a pool "heavier" than the all-pool average must be accompanied by a flux from a "lighter" pool. What is important here is the perturbation in the respired $\delta^{13}C$ due to the slowly decreasing atmospheric $\delta^{13}C$. As long as the biosphere remains the same, that is, $f_k(x, y, t_s)$ has not changed with time, then what matters to the atmospheric $\delta^{13}C$ signature is how the atmospheric $\delta^{13}C$ perturbation is propagated through the biospheric pools. This is derived formally below.

At each location (x, y), let us split the $\delta^{13}C$ of a biospheric pool k into a seasonally varying equilibrium component $\delta_{k0}(t_s)$ and a perturbed component $\delta'_k(t_s, t)$:

$$\delta_{b,k}(t_s, t) = \delta_{k0}(t_s) + \delta'_k(t_s, t) \tag{11}$$

Let us further split the equilibrium component into $< \delta_{b0}(t_s) >$, the pool-integrated mean, and $\delta^*_{k0}(t_s)$, the departure of each pool from the all-pool average:

$$\delta_{k0}(t_s) = < \delta_{b0}(t_s) > + \delta^*_{k0}(t_s) \tag{12}$$

where $< \delta_{b0}(t_s) >$ is the flux-weighted mean $\delta^{13}C$ across the pools:

$$< \delta_{b0}(t_s) > = \sum_k f_k(t_s)\delta_{k0}(t_s) \tag{13}$$

It follows from equations (12) and (13) that

$$\sum_k f_k(t_s)\delta^*_{k0}(t_s) = 0 \tag{14}$$

so that equation (11) becomes

$$\delta_{b,k}(t_s, t) = < \delta_{b0}(t_s) > + \delta^*_{k0}(t_s) + \delta'_k(t_s, t) \tag{15}$$

Substituting equation (15) into equation (10) and applying the conditions $\sum_k f_k(t_s) = 1$, we obtain:

$$\begin{aligned} \delta_b(t_s, t) &= \sum_k f_k(t_s)\delta_{b,k}(t_s, t) \\ &= < \delta_{b0}(t_s) > \sum_k f_k(t_s) + \sum_k f_k(t_s)\delta^*_{k0}(t_s) \\ &\quad + \sum_k f_k(t_s)\delta'_k(t_s, t) \\ &= < \delta_{b0}(t_s) > + \sum_k f_k(t_s)\delta'_k(t_s, t) \end{aligned} \tag{16}$$

In other words, from the atmospheric perspective, the $\delta^{13}C$ contributions from initial or steady variations in $\delta^{13}C$ amongst all the pools cancel, and the critical parameter is the temporal evolution of the $\delta^{13}C$ of each pool.

The above conclusion hinges on the assumption that $f_k(t_s)$, the relative contribution from each pool, has not changed in time. It is difficult to evaluate this assumption. Changes in $f_k(t_s, t)$ may result from changes in the sizes of the different pools due to carbon sequestration, as well as from changes in climate-sensitive transfer rates. The error is small as long as $f_k(t_s, t) - f_k(t_s, 0)$ is small.

5.1. Age Versus Turnover Time

To estimate $\delta'_k(x, y, t_s, t)$, the departure from the initial equilibrium, one needs to know, on average, when the plant material was formed and $\delta_A(t_{formation})$, the atmospheric $\delta^{13}C$ at the time of formation. The history of δ_A is known from atmospheric measurements. If we assume that $\Delta(x, y, t_s)$ has not changed over time, this reduces to the determination of τ_k, the mean age of the carbon in biospheric compartment k when it is returned to the atmosphere.

Here we distinguish between turnover time and the mean age in the estimation of τ_k [*Bolin and Rodhe*, 1973; *Rodhe*, 1992]. For each litter or soil pool, the transfer of carbon amongst the pools is not sequential. Carbon from one pool may be transferred, at different rates, to several pools (compare Figure 6). Similarly, carbon entering a pool may come from multiple sources, namely, the microbial compartment. Turnover time is the quotient of the pool size divided by the sum of the outgoing fluxes. The turnover time expresses how long a carbon molecule spends in the reservoir before it leaves. It contains no information about how long the carbon molecule entering the pool has been in the biosphere, that is, since it left the atmosphere. Age, however, takes into account the carbon entering and leaving the pool. Take the microbial pool as an example. The pool size is small, and the turnover time is short. The use of a turnover time to determine $\delta_A(t - \tau)$ would have implied ^{13}C of recent origin. However, the microbial pool receives carbon from several pools including the slow and old soil organic pools. Thus, although the old carbon does not stay long in the microbial pool, the respired carbon reflects the long residence time in the entire biosphere.

We start the age calculation with the turnover times of live biomass derived from the Frankfurt Biosphere Model [*Lüdeke et al.*, 1994]. Turnover times of live leaves and roots range between 1 (in deciduous regions) and 8 years (in boreal forest), while those of live wood range between 0 (in grasslands) and 60 years (in temperate deciduous and evergreen forests). The turnover times of the live leaves and roots are treated as the initial ages of the surface metabolic and structural pools, and those of live wood are treated as the initial ages of the woody litter pools. We then followed, in CASA, the carbon from the litter pools to the other soil pools and computed the resultant age of each compartment as a uniform mixture after accounting for the incoming and outgoing fluxes.

Table 1a shows the annual mean flux fractions, turnover times, and ages for the different compartments of the ecosystems. Within each ecosystem, the shortest turnover times are $\leq$0.5 years for the surface and soil metabolic pools, which contribute ~6% of the total respired CO_2 for broad-leaved and needle-leaved forests to ~46% for cultivation. Turnover times are $\leq$1.5 years for the surface and soil microbial pools, which contribute ~25% of the total respired CO_2 for all ecosystems. Similarly, turnover times are ~5 years for the woody litter pool, which contributes ~13% of the respired fluxes for all forest ecosystems. The slow pools, which contribute ~25 and 18% for forests and grasslands, respectively, have turnover times that range from ~10 years in the tropics to ~25 years for needle-leaved deciduous forests. The passive, or armored, pool has the longest turnover time, >400 years, but contributes <0.5% of the total respired flux for all ecosystems. The flux-weighted turnover times, dominated by the 25% from the slow pools, are 3–12 years. The flux fractions and turnover times modeled here by CASA are comparable to those obtained by *Schimel et al.* [1994] using the model CENTURY, though our estimates of the microbial contributions are lower by ~5–10%.

The difference between age and turnover times for each pool is clear in Table 1a. Large differences, ~40 years, are found for the woody litter pools of forest ecosystems and reflect the longevity of trees. Differences >20 years are also found downstream of the woody litter compartment in the surface and soil microbial, slow and passive compartments. The woody litter and microbial pools contribute over 60% of the respired flux from forest ecosystems. The resultant flux-weighted ages of the respired CO_2 range from 25 to 35 years for forest ecosystems and from 7 to 15 years for herbaceous vegetation. These are larger than the corresponding turnover times by factors of >4 and >2 for forest and herbaceous ecosystems, respectively.

Because δ_A changed very little prior to the preindustrial era, ~200 years ago, there is no variation in the δ_b of respired carbon older than 200 years. Hence the "effective δ^{13}C age" of any pool, that is, the age important for estimating the δ_b of the respired carbon, cannot exceed 200 years. We found that the "effective δ^{13}C age" equals the chronologic age for all pools except for the passive (armored) pool and the soil microbial and slow pools which receive carbon from the passive pool. The "effective δ^{13}C ages" are ~10 and 5% lower than the chronologic ages for the latter two pools, which contribute ~15 and 25% of the total respired fluxes, respectively. These differences have a small impact on the δ^{13}C of the respired CO_2, and we therefore consider the two ages equivalent.

Ciais et al. [1995a,b] obtained the turnover times and relative flux contributions of the various pools from *Schimel et al.* [1994] and added an average turnover time of 16 years for the above ground biota to estimate the δ_b of the respired carbon. Their δ_b estimate used ~5 years for the tropical rainforest and ~200 years for the tundra. Their low estimate compared to ours reflects the use of turnover times rather than ages in their calculation.

With the recent atmospheric δ^{13}C trend of $-0.02‰\ yr^{-1}$, an error of 10 years in the age of the total respired CO_2 would translate into an error of $-0.2‰$ in the respired δ_b. This is the case with the microbial pools which contribute ~30% to the total respired flux. Our use of an age of ~25 years instead of a turnover time of <1 year makes this pool a significant contributor to $\mathcal{D}_b$ and increases the value of $\mathcal{D}_b$ by ~0.15‰ ($= 0.02‰ yr^{-1} \times (25\text{-}1) yr \times 30\%$).

5.2. Seasonality of the Respired δ^{13}C

Once the ages τ_k are known, $\delta_{b,k}(x, y, t_s, t)$ can be estimated from the history of the atmospheric δ^{13}C, and the δ_b of the respired carbon can be estimated as the flux - weighted sum of the contributions from the nine biospheric pools.

The seasonality of respiration is determined by temperature, moisture, and the timing of litter inputs [*Randerson et al.*, 1996]. The relative contribution of respiration flux from each pool $f_k(x, y, t_s)$ also varies seasonally, reflecting differences in the controls on decomposition from different pools as well as variations in litterfall and pool sizes. Therefore the $\tau(x, y, t_s)$ and δ_b of the total respired flux vary seasonally as well.

The seasonal range of the respired δ^{13}C, as modeled by CASA, is $\leq 0.3‰$ everywhere (not shown) and is smaller by factors of 10 to >50 than the seasonal range in Δ. This is because the seasonal range of the respired δ^{13}C is bounded by the maximum age of the respired CO_2 and the recent trend in atmospheric δ_A. For most vegetation, the surface and soil metabolic pools and microbial pools together contribute ~75% of the total respired CO_2 (compare Table 1a). Consider the following typical values. Let the contributions by the metabolic litter and microbial pools be 60 and 15%, respectively, in the winter and 25 and 50%, respectively, in the summer. The remaining pools would thus contribute a constant 25% of the total respiration throughout the year. If we take the ages of the metabolic and microbials pools to be 1 year and 30 years, respectively, then the seasonal part of the respired CO_2 has an age of 5.1 years ($= .60 \times 1 + .15 \times 30$) in the winter and 15.25 years ($= .25 \times 1 + .50 \times 30$) in the

summer. With an observed δ_A trend of $-0.02‰$ yr^{-1}, a seasonal age difference of 10 years translates into a $\delta^{13}C$ range of $0.2‰$.

5.3. Variations in the Isotopic Disequilibrium

The decreasing trend in atmospheric δ_A implies an isotopic disequilibrium between the photosynthetic and respiratory fluxes even though the total CO_2 fluxes are balanced in the annual mean. It is convenient to rewrite equation (1b) to include the isotopic disequilibrium $\mathcal{D}_b$:

$$\begin{aligned} C_a\frac{\partial}{\partial t}(\delta_a) + C_a T(\delta_a) &= -\Delta \times F_{ap} + (\delta_b - \delta_A) \times F_{ba} \\ &= -\Delta \times F_{ap} + (\mathcal{D}_b - \Delta) \times F_{ba} \end{aligned} \tag{17}$$

where

$$\begin{aligned} \mathcal{D}_b(x,y,t_s,t) &= \delta_b(x,y,t_s,t) - \delta_A(t_s,t) + \Delta(x,y,t_s) \\ &= -\widetilde{\Delta}(x,y) + \Delta(x,y,t_s) \\ &\quad +[\delta_A(t_s, t - \tau_{age}(x,y,t_s)) - \delta_A(t_s,t)] \end{aligned} \tag{18}$$

and in the annual mean

$$\widetilde{\mathcal{D}_b}(x,y,t) = \widetilde{\delta_A}(t - \tau_{age}(x,y,t)) - \widetilde{\delta_A}(t) \tag{19}$$

We calculated the $\mathcal{D}_b$ for 1988 when the atmospheric $\delta_A = -7.8‰$ (Plate 2). The flux-weighted annual mean $\widetilde{\mathcal{D}_b}$

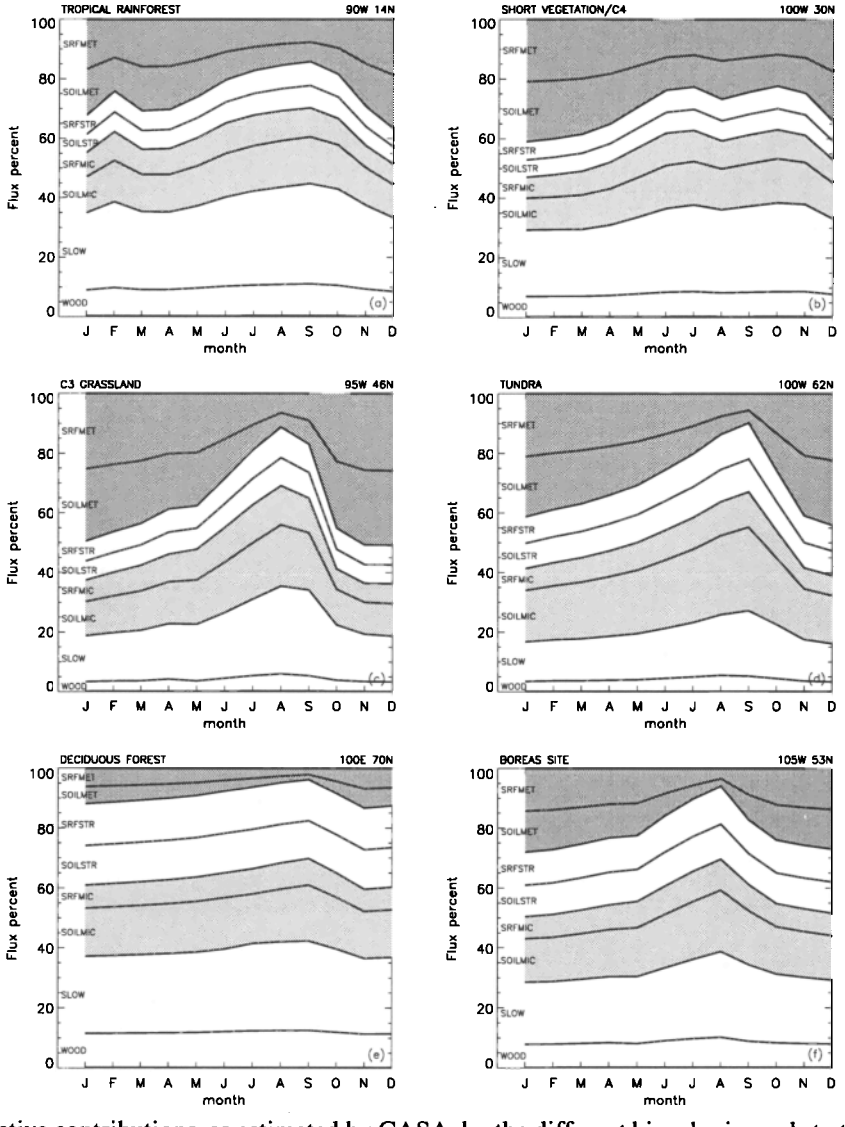

Figure 7. Relative contributions, as estimated by CASA, by the different biospheric pools to the monthly mean respired CO_2 flux at (a) tropical rainforest (90°W, 14°N), (b) short vegetation, C_4 grassland (100°W, 30°N), (c) C_3 grassland (95°W, 46°N), (d) tundra (100°W, 62°N), (e) deciduous forest (100°E, 70°N), and (f) boreas field site (105°W, 53°N)

(t = 1988) for the globe is 0.33‰. $\widetilde{\mathcal{D}_b}$ is ~0.45‰ in the tropical rainforest and is >0.5‰in the boreal forests. The lowest value of $\widetilde{\mathcal{D}_b}$, ~0.2‰, is found in grasslands and deserts. Our global value is much less than the value 0.43‰ derived from *Francey et al.*'s [1995] G_b $\widetilde{\mathcal{D}_b}$ of 25.8 Gt ‰yr^{-1} and G_b of 60 Gt C yr^{-1}. The *Francey et al.* [1995] value is based on calculations by *Enting et al.* [1995], using *Emanual et al.*'s [1981] six-box model with air and ice core δ^{13}C data.

To investigate the importance of the above ground woody lifetimes on the $\mathcal{D}_b$ distribution, we carried out a separate integration (termed the "no tree" vegetation) of CASA wherein we set to zero the initial ages of the litter (i.e., the ages of the live woody biomass). The neglect of the longevity of trees yields a global flux-weighted mean disequilibrium of 0.20‰, the value employed by *Keeling et al.* [1989b] and *Tans et al.* [1993].

Figure 8 shows the latitudinal distributions of the zonally averaged annual mean $\widetilde{\mathcal{D}_b}$ (y,t), as calculated for t = 1988 for the "actual" and "no-tree" vegetation distributions. The latitudinal distributions reflect principally the distributions of forests versus herbaceous vegetation, with secondary influences of climate. The distribution for the current vegetation shows two relative maxima, one for the tropical forests and the other for the middle- to high-latitude forests, with the larger maximum in the cooler climate. $\widetilde{\mathcal{D}_b}$ decreases toward the polar latitudes because the tundra has little woody vegetation, and the long-lived pools contribute little to the total respired flux from the tundra. The $\widetilde{\mathcal{D}_b}$ profile for the no-tree distribution clearly shows the influence of climate on decomposition rates, with larger $\widetilde{\mathcal{D}_b}$ at higher latitudes.

The distribution of $\mathcal{D}_b$ modeled in this study is different from those used in other studies where either $\mathcal{D}_b$ is assumed constant across latitudes [*Keeling et al.*, 1989a], or $\mathcal{D}_b$ is estimated to be larger at high latitudes because of the longer turnover time of carbon in the soils [*Ciais et al.*, 1995a]. The significance of the $\mathcal{D}_b$ distribution on atmospheric δ^{13}C is explored below.

The seasonal variations of $\mathcal{D}_b(x,y,t_s,t)$ (not shown) reflect mainly the seasonality of $\Delta(x,y,t_s)$ (compare equation (18)), since the seasonal range of $\Delta(x,y,t_s)$ can be as large ~5–10‰ at middle- to high-latitudes and can overwhelm the seasonal variations in δ_A(<1‰). Indeed, at midlatitudes, $\mathcal{D}_b(x,y,t_s,t)$ reaches large negative values in winter months with minimum Δ. The transient negative values underline the separate processes and separate carbon pools involved in photosynthesis and respiration. The winter contributions to the annual mean $\widetilde{\mathcal{D}_b}$ remain negligible because winter fluxes are small.

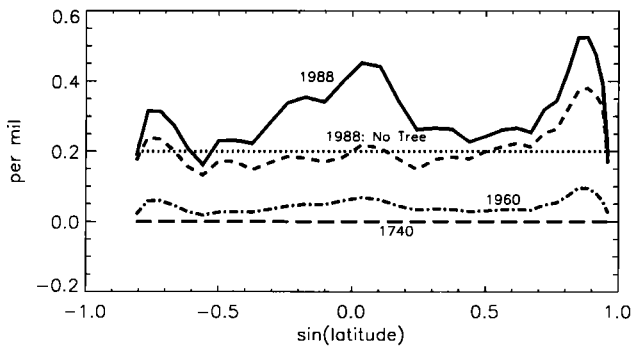

Figure 8. Latitudinal distributions of the zonally averaged $\mathcal{D}_b$ (isotopic disequilibrium) for the seven experiments. The "1988" distribution (solid curve) was used in experiments 1 and 4; the constant (=18.6) value (dotted curve) was used in experiments 2 and 3. The "1988: no-tree" distribution (short-dashed curve) was used in experiment 5. Experiments 6 (dashed-dotted curve) and 7 (long-dashed curve) employed the "1960" and "1740" distributions, respectively.

6. Atmosphere Signature

To investigate the atmospheric δ^{13}C variations resulting from the background biosphere with ^{12}C-flux equilibrium, we employ the global three - dimensional tracer transport model developed at GISS [e.g., *Russell and Lerner*, 1981; *Fung et al.*, 1983, 1987, 1991; *Tans et al.* 1990] to redistribute the carbon in the atmosphere (equation (1b)). In equations (1a) and (1b), $\mathcal{T}$ is the atmospheric transport operator and includes large-scale advection by winds as well as subgrid mixing by moist and dry convection. In the version of the tracer model employed here, they are derived from winds every four hours and circulation statistics from the GISS atmospheric general circulation model [*Hansen et al.*, 1983].

In the tracer model, geographically and temporally varying sources and sinks of CO_2 and δ^{13}C are prescribed at the surface. For each source/sink, the three-dimensional (3-D) model was integrated separately for its ^{12}C and ^{13}C signature in the atmosphere. The individual responses are then combined to yield the total response. Here, to focus on the effects of isotopic exchange on δ^{13}C variations in the atmosphere, we take F_{ap} and F_{ba}, the photosynthetic and respiratory CO_2 fluxes, respectively, from *Fung et al.* [1987], where the fluxes have been tuned to produce in the same 3-D tracer transport model, atmospheric CO_2 seasonalities that resemble those observed in the northern hemisphere. The seasonal ^{12}C fluxes produce an annual-mean north-south CO_2 gradient of ~0.5 ppmv in the atmosphere, even in the absence of net sources or sinks in the annual mean.

We carried out seven experiments to investigate the sensitivity of the atmospheric δ^{13}C signature to different assumptions about Δ and $\mathcal{D}_b$. Experiment 1 is the control; experiments 2-4 investigate the sensitivity of the atmospheric δ_a signature to geographic variations in Δ and $\mathcal{D}_b$. Experiment 5 explores the variations in δ_a due to assumptions about the age of live woody biomass. Experiments 6 and 7 explore changes in δ_A(Table 2).

Experiment 1 uses the full spatial and seasonal variations of $\Delta(x,y,t_s)$ and $\mathcal{D}_b(x,y,t_s,t$ = 1988) as calculated by

Table 2. List of Tracer Model Experiments

Experiment	Vegetation	Year	δ_A, ‰	Discrimination Δ	Disequilibrium $\mathcal{D}_b$
1	current	1988	-7.8	SiB2 (x, y, t_s)	CASA(x, y, t_s)
2	current	1988	-7.8	18.6‰	0.2‰
3	current	1988	-7.8	18.6‰	CASA (x, y, t_s)
4	current	1988	-7.8	SiB2 (x, y, t_s)	0.2‰
5	current, no tree	1988	-7.8	SiB2 (x, y, t_s)	CASA (x, y, t_s)
6	current	1960	-7.0	SiB2 (x, y, t_s)	CASA (x, y, t_s)
7	current	1740	-6.3	SiB2 (x, y, t_s)	CASA (x, y, t_s)

SiB2-GCM and CASA for the actual vegetation distribution. Experiment 2 assumes globally uniform Δ and $\mathcal{D}_b$. A value of $\Delta = 18.6$ ‰ provides ^{13}C equilibrium between an initial atmospheric δ_A of -6.4‰ and a biospheric δ_b of -25‰. The value of $\mathcal{D}_b = 0.2$‰ is commonly used in carbon budget calculations [*Quay et al.*, 1992; *Tans et al.*, 1993]. In experiment 3, Δ is geographically uniform, with a value of 18.6‰; $\mathcal{D}_b$, calculated by CASA, is spatially, and to a small degree, seasonally varying as in experiment 1. Experiment 4 employs the varying Δ calculated by SiB2-GCM but a uniform $\mathcal{D}_b = 0.2$‰. Comparison of experiments 1 and 3 will quantify the importance of Δ variations while comparison of experiments 1 and 4 will quantify the importance of $\mathcal{D}_b$ variations. Experiment 5 is like experiment 1 but uses the $\mathcal{D}_b(x, y, t_s, t = 1988)$ distribution for the no-tree rather than the actual vegetation distribution. Thus $\mathcal{D}_b$ reflects mainly the turnover times rather than ages of the carbon in the soils. Experiments 6 and 7 are like experiment 1 but are for $\delta_A = -7.0$‰ in 1960 and for $\delta_A = -6.4$‰ in 1740 rather than $\delta_A = -7.8$‰ in 1988. To isolate the effects of biospheric isotopic variations on atmospheric $\delta^{13}C$, we have used the same F_{ap} and F_{ba} for experiments 1–7, even though it is likely that photosynthesis and respiration rates for 1988 would be different from those in the earlier period.

For each experiment, we integrate equations (1a) and (1b) for 3 years. Results presented below are from the third year of the integrations. Equation (1b) requires information about C_A. Here, to isolate the relative contributions of biospheric exchanges to the total atmospheric δ_A variations, we use, where possible, observed values of C_A on the left-hand side in equation (1b). For the global analysis, we add the global distribution of C_A simulated for scenario 7 of *Tans et al.* [1990] to a uniform background CO_2 concentration, as this distribution includes all the CO_2 sources and sinks and obtains reasonable agreement with the available atmospheric and oceanic observations. Like *Fung et al.* [1991], we compare the observations with the simulation at the grid boxes containing the observation sites, except at Point Barrow where the grid box north of Point Barrow is used to be compatible with the measurements from the "clean-air" sector.

6.1. Seasonal Cycles

Three examples illustrate how $\mathcal{D}_b$ and seasonal Δ can affect the seasonal fluxes. Consider two locations with the seasonal fluxes shown in Figure 9. The seasonal fluxes, F_{ap} and F_{ba} are totally out of phase at site 1 and in phase at site 2 (Figures 9a,b). In example 1 (Figures 9c,d), Δ is constant in time, and both sites are in ^{13}C equilibrium. The seasonal amplitudes in $\delta^{13}C$ would be $\mathcal{A}_1 = |\Delta \times F_{ba}|$ for site 1 and $\mathcal{A}_2 = 0$ for site 2. In example 2 (Figures 9e,f), ^{12}C and ^{13}C equilibria still obtain, but we let Δ be seasonal, with a summer maximum. Both $\mathcal{A}_1$ and $\mathcal{A}_2$ are increased compared to example 1. Example 3 (Figures 9g,h) considers a biosphere with ^{12}C but not ^{13}C equilibrium. Let Δ be seasonally invariant. The addition of the isotopic disequilibrium $\mathcal{D}_b$ reduces the contrast between the ^{13}C fluxes into and out of the biosphere at site 1, reducing $\mathcal{A}_1$. It also removes the cancellation between the fluxes at site 2, increasing $\mathcal{A}_2$. The examples illustrate that seasonality of $\delta^{13}C$ at a particular site is affected not only by the phasing of Δ but also by the magnitude of $\mathcal{D}_b$.

In experiment 1, the simulated amplitude in δ_a is ~0.9‰ at Point Barrow, Alaska, and is ~0.35‰ at Mauna Loa, Hawaii (Plate 3). The maximum δ_a simulated is in August at Point Barrow and in September at Mauna Loa, close to those observed. The southward decrease of the δ_a seasonal cycle mirrors the decrease in CO_2 amplitudes. This is clear in experiment 2, where both Δ and $\mathcal{D}_b$ are constants. The largest effects on the δ_a amplitude are the magnitudes and relative phasing of the photosynthetic and respiratory fluxes. Amplitudes are as large as 1.2‰ in inland regions, where not only the CO_2 but also the Δ seasonalities are strong (Plate 4). The simulated seasonal cycles at the northern hemisphere sites are reduced in experiments 2 and 3 but relatively unchanged in experiment 4, compared to experiment 1, demonstrating the influence of the Δ seasonality. Seasonality in δ_b is small and contributes little to the atmospheric seasonal variations. This is illustrated by the comparison of the seasonal amplitudes in experiments 1 and 4. For the same F_{ap}, the summer maximum in Δ at high latitudes results in reduced ^{13}C removal and hence a "heavier" atmosphere, compared to experiment 3 with an aseasonal Δ. Because $\Delta(t_s)$ and $F_{ap}(t_s)$

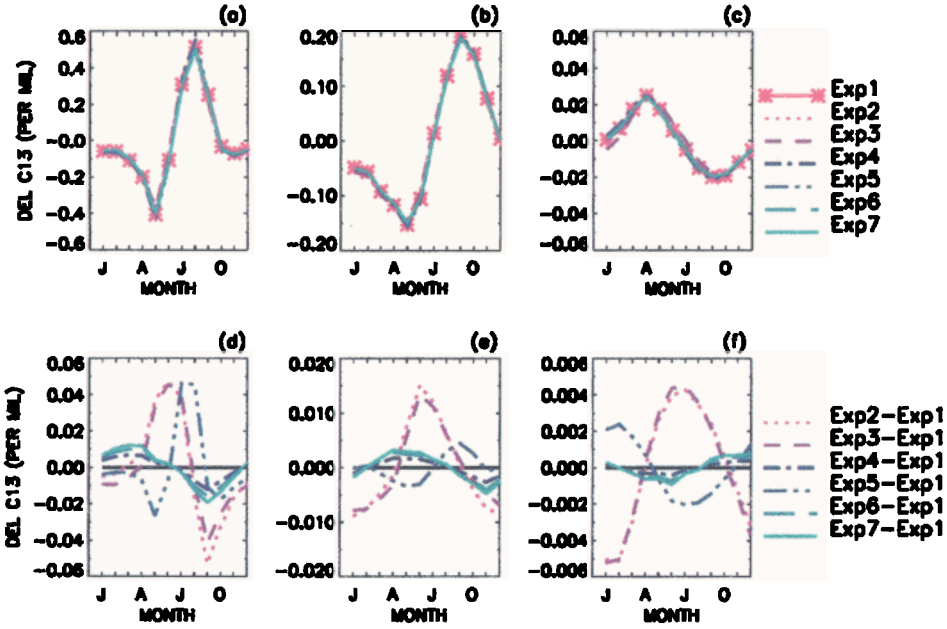

Plate 3. Seasonal cycle of atmospheric $\delta^{13}C$ simulated in the vicinity of (a) Point Barrow, Alaska, (b) Mauna Loa, Hawaii, and (c) the south pole for experiments 1-7. The $\delta^{13}C$ in the model grid box north of Point Barrow is used to represent the clean-air sector of the stations, (d)-(f) the departure of the $\delta^{13}C$ in each experiment from those in experiment 1 are shown.

are not exactly in phase, the $\delta^{13}C$ seasonal cycle at middle- to high-latitudes lags behind the corresponding CO_2 cycle seasonal cycles. The lag is small, < 1 month, and may not be detectable. The value Δ has a summer minimum around 40°N (Plate 1), which would reduce the summer contrast in atmospheric $\delta^{13}C$ between photosynthesis and respiration. While the Δ seasonality is clearly enhancing the atmospheric $\delta^{13}C$ cycle at Point Barrow, its effects are diminished at Mauna Loa, owing both to dilution and to competition from the opposing Δ seasonality at other latitudes.

The seasonal cycles in experiment 5 (no-tree vegetation) are in phase with those in experiment 1 but are greater in amplitude by ~10% at the observing sites.

Experiments 1, 6, and 7 differ only in the value of the atmospheric δ_A and hence $\mathcal{D}_b$. The seasonal cycles simulated in experiment 6 (1960 δ_A) are smaller than those in experiment 1 (1988) by ~0.02‰ or ~1.7% of the amplitude in experiment 1. These experiments suggest that we should expect a positive trend of 0.06% yr^{-1} in the $\delta^{13}C$ amplitudes owing only to the recent atmospheric δ_A trend of -0.02‰ yr^{-1}. However, the CO_2 amplitude at Point Barrow has been observed to have a positive trend of ~1.3% yr^{-1} in the past 35 years [*Keeling et al.*, 1995], about 20 times larger than that due to $\mathcal{D}_b$. Our experiments thus show that, for the recent decrease rate of δ_A in the atmosphere, changes in biospheric dynamics dominate the signal in δ_A amplitude trends

6.2. Annual Mean Distributions

In general, the simulated δ_a gradient for the NOAA sampling sites is very small and within ±0.03‰ of zero (Plates 5a and b). In these experiments, which include only exchanges with the background biosphere, the jaggedness of the simulated latitudinal profiles at the monitoring stations mirrors the jaggedness of the CO_2 profiles and registers the degree of continental influence at each station. This is seen clearly in Plate 6a, where annual mean $\delta^{13}C$ can be as large as ±0.06‰ relative to the south pole.

The geographic variations of photosynthetic discrimination Δ have minimal influence on the annual-mean latitudinal gradient of atmospheric $\delta^{13}C$, unlike the case for the atmospheric $\delta^{13}C$ seasonal cycles. This can be seen in the comparison of the results of experiments 1 and 3 (Plate 5b), where the northern hemisphere difference in δ_a is <0.005‰. This is not surprising, as Δ multiplies both F_{ap} and F_{ba} in equation (17), and its effects are approximately canceled in the annual mean for a biosphere whose ^{12}C fluxes balance.

The hemispheric difference in the annual-mean δ_a in the atmosphere is dependent on the latitudinal gradient in $\widetilde{\mathcal{D}_b}$, the isotopic disequilibrium between the photosynthetic and respiratory fluxes. The differences in the hemispheric gradients are very small, ~−0.003‰, between experiments 1 and 3 which use the $\mathcal{D}_b$ simulated by CASA (Plate 5b) Ex-

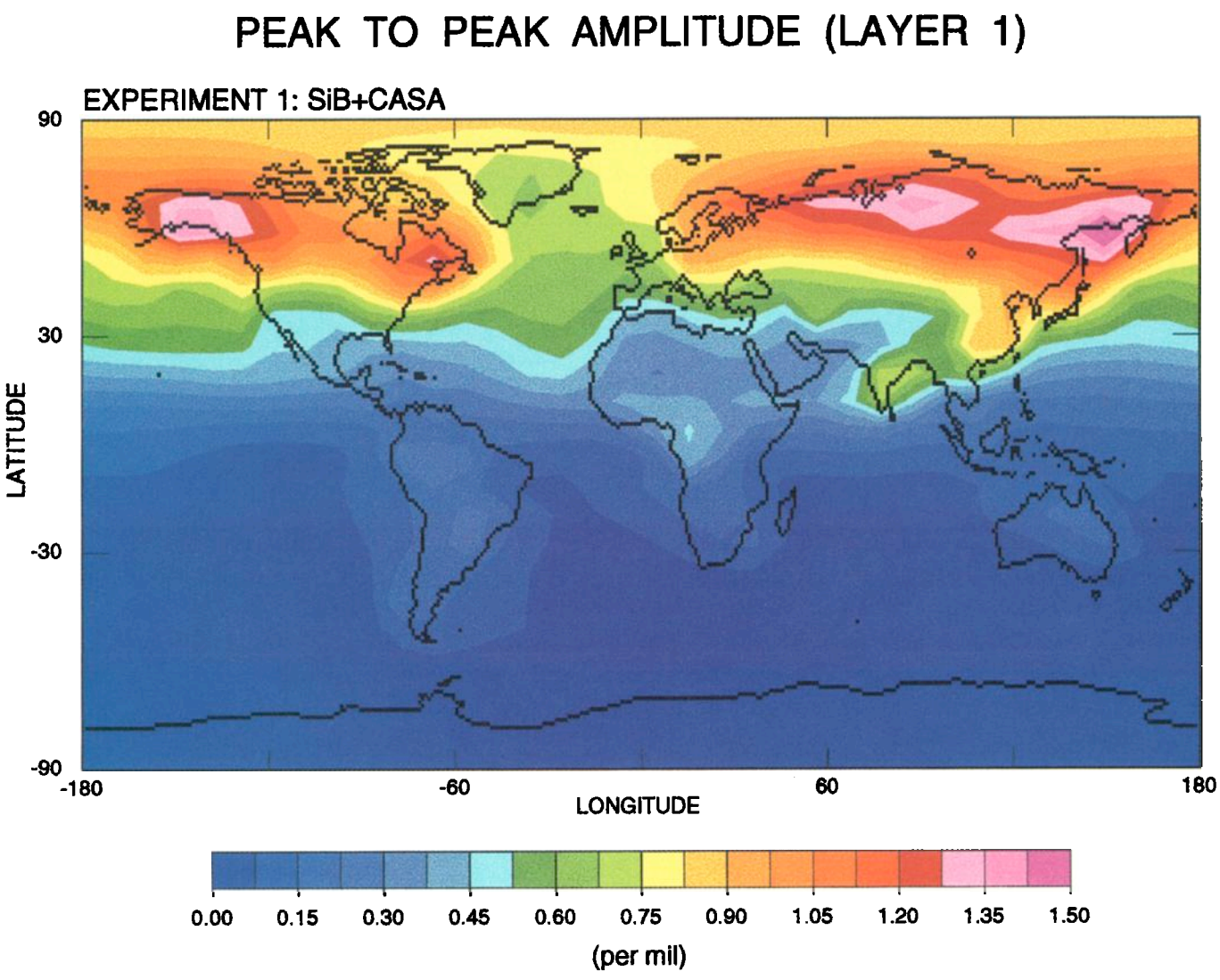

Plate 4. Global distribution of the seasonal range (in per mil) of atmospheric $\delta^{13}C$ simulated for experiment 1.

periments 2 and 4, which employ a constant $\mathcal{D}_b = 0.2‰$, obtain latitudinal gradients which are slightly steeper, by $\sim -0.0015‰$, than in experiment 1. Similarly, the gradients in experiment 5 for the no-tree vegetation with smaller $\mathcal{D}_b$ are even steeper, by $\sim -0.01‰$, than in experiment 1. The steepest gradient is simulated for experiment 7 for 1740, when $\mathcal{D}_b = 0$. Plate 2 shows that a greater $\mathcal{D}_b$ means the addition of "heavier" carbon to the northern atmosphere. This result, that the δ_a hemispheric difference steepens with decreasing $\mathcal{D}_b$, appears counterintuitive.

For gross CO_2 exchange between the atmosphere and biosphere, another factor that contributes to an annual mean atmospheric δ_a gradient is the rectifier effect [*Denning et al*, 1995]: an annual mean atmospheric CO_2 gradient results because the withdraw of photosynthetic carbon is from a deeper (summer) atmospheric boundary layer than the addition of respiratory carbon. This net positive CO_2 concentration at a fixed height in the lower troposphere yields a negative $\delta^{13}C$ signature, since biosphere carbon is "lighter" than atmospheric carbon. Plate 6b shows the surface distribution of the annual mean atmospheric $\delta^{13}C$ simulated for the year 1740, when the system was assumed to be in ^{13}C balance or $\mathcal{D}_b = 0$. The variations in δ_a mirror the variations in the annual mean CO_2 distribution in this model. The annual mean δ_a is negative (positive) where the CO_2 mean is positive (negative). As the mean CO_2 gradient is positive (higher in the northern hemisphere) in this model, the $\delta^{13}C$ gradient is negative, the hemispheric difference being $\sim -0.04‰$. Locally, $\delta^{13}C$ can be as large as $-0.1‰$ at high latitudes where the annual mean CO_2 exceeds the south pole value by x1.5 ppmv. Plate 6c shows the difference between the $\delta^{13}C$ annual mean simulated in experiment 1 and that in experiment 7 (1740), that is, the difference due to $\mathcal{D}_b$ alone. If no atmospheric CO_2 gradient resulted from the gross CO_2 exchanges, we would expect the companion $\delta^{13}C$ gradient to be positive and to reflect the age difference be-

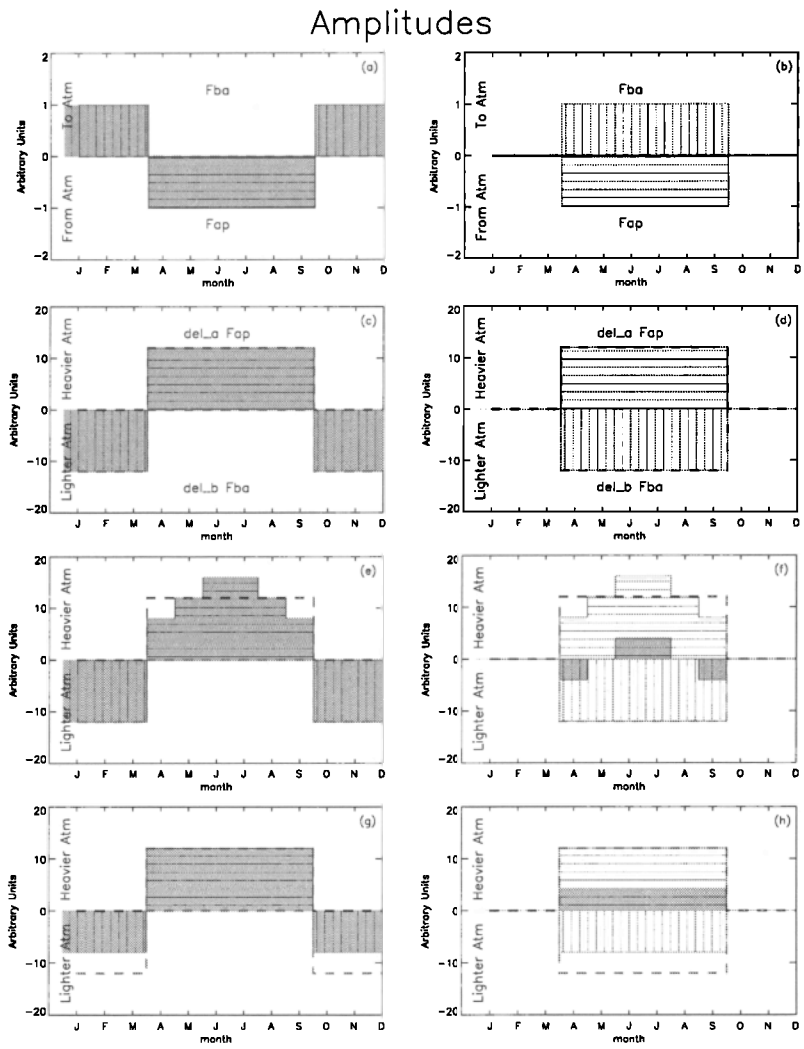

Figure 9. Examples illustrating the effects of Δ seasonality and $\mathcal{D}_b$ on the seasonality of the ^{13}C fluxes. Seasonal CO_2 fluxes are shown in the first row for two sites: where F_{ap} and F_{ba} are equal in magnitude and out of phase (left column) and equal in magnitude but in phase (right column). The impact on ^{13}C fluxes at each site when the CO_2 fluxes in the first row are combined with constant Δ and zero $\mathcal{D}_b$(second row), seasonality in Δ and zero $\mathcal{D}_b$ (third row), and constant Δ and $\mathcal{D}_b \neq 0$ (fourth row) are shown in the corresponding column. Vertical bars (horizontal lines) indicate fluxes that increase (decrease) atmospheric CO_2 or $\delta^{13}C$. Shaded regions indicate the imbalance between the incoming and outgoing fluxes. The dashed lines in Figures 9c–9h reproduce the fluxes in Figures 9c and 9d, the reference cases.

tween the photosynthetic and respired carbon. Experiment 1 would produce a positive δ_a gradient of $\sim 0.025‰$ between the hemispheres in the absence of a CO_2 gradient (Plate 6c). The corresponding difference would be ~ 0.015 and $\sim 0‰$ for 1960 and 1740 (experiments 6 and 7), respectively.

A positive mean CO_2 gradient implies an excess of respired carbon with $\delta^{13}C \sim -24.5‰$ over some fixed depth in the boundary layer in the northern hemisphere. The excess of biospheric ("light") carbon depresses the northern hemisphere δ_a relative to the south. This is also seen clearly in the δ_a profile (the "background" $\delta^{13}C$ gradient) simulated in experiment 7 (Plate 5a), which has no isotopic disequilibrium. The "background" $\delta^{13}C$ hemispheric difference in this model is $\sim -0.03‰$. The δ_a gradient due to $\mathcal{D}_b$ is then added to the negative $\delta^{13}C$ background gradient. We speculate that the atmospheric model of [*Denning et al.*, 1995], which produces a larger CO_2 north-south gradient, $\sim$ 2 ppmv, for the same biospheric fluxes, would produce a negative $\delta^{13}C$ gradient in the atmosphere.

The latitudinal profiles of δ_a for experiments 1 and 5 (for current and no tree vegetation distributions) show little difference even though the globally averaged $\mathcal{D}_b$ for the two experiments are different by a factor of 1.5. This is because the largest difference in $\mathcal{D}_b$ between the two experiments is in the tropics, and tropical sources and sinks in general have negligible expression in atmospheric concentration dif-

ferences between the hemispheres. The global difference in $\mathcal{D}_b$ between the two experiments (0.33 and 0.2‰ for experiments 1 and 5, respectively) is significant for the global carbon budget.

7. Implications for the Contemporary Carbon Budget

In this paper, two dynamic carbon models, SiB2-GCM and CASA, were employed to determine the geographic and seasonal variations of Δ, photosynthetic discrimination, and $\mathcal{D}_b$, the isotopic disequilibrium between the fixed and respired carbon. The global flux-weighted Δ is between 12 to 13 and 15.7‰, and the global, flux-weighted $\mathcal{D}_b$ is 0.33‰ for 1988. The $\mathcal{D}_b$ for no-tree vegetation is 0.2‰ for 1988.

The upper limit of Δ includes a middle-of-the-road assumption about the areal extent of C_4 vegetation. The lower limit includes fractionation during the final diffusion step to the carboxylation sites. Our lower limit is significantly lower than the value of Δ = 18‰ commonly used in carbon budget studies [*Quay et al.*, 1992; *Tans et al.*, 1993].

The no-tree $\mathcal{D}_b$ value of 0.2‰ is the same as those used in other investigations [*Keeling et al.*, 1989a; *Quay et al.*, 1992; *Tans et al.*, 1993; *Ciais et al.*, 1995a,b]. However, we do not consider this $\mathcal{D}_b$ realistic, as it neglects the time a ^{13}C molecule spends in live woody biomass.

To investigate the sensitivity of the global carbon budget to our new estimates of Δ and $\mathcal{D}_b$, we employ the ^{12}C and ^{13}C mass balance equations, following *Tans* [1980], *Tans et al.* [1993], and *Francey et al.* [1995]:

$$\frac{\partial}{\partial t}(C_A)|_{total} = S_{FF} + S_{DEF} + F_{ao} + F_{oa} + F_{ap} + F_{ba}. \quad (20)$$

$$\begin{aligned} C_A \frac{\partial}{\partial t}(\delta_A)|_{total} &= (\delta_{FF} - \delta_A) \times S_{FF} \\ &+ (\delta_{DEF} - \delta_A) \times S_{DEF} \\ &+ \mathcal{D}_b \times G_b - \Delta \times N_b \\ &+ \mathcal{D}_o \times G_o + \epsilon_{ao} \times N_o \end{aligned} \quad (21)$$

The change in the abundance of carbon and its isotopes in the atmosphere is equal to the sum of the changes due to releases from fossil fuel combustion (S_{FF}), land use modification (S_{DEF}), atmosphere-ocean exchanges (F_{ao} and F_{oa}), and atmosphere-biosphere exchanges. In equation (21), $G_o(= F_{oa})$ and $G_b(= F_{ba})$ are the gross exchanges with the ocean and biosphere, respectively, and $N_o(= F_{ao} + F_{oa})$ and $N_b(= F_{ap} + F_{ba})$ are the net fluxes or the sinks for anthropogenic CO_2 sought. $\mathcal{D}_o$ is the isotopic disequilibrium associated with atmosphere-ocean exchange, and ϵ_{ao} is the fractionation coefficient associated with CO_2 invasion to the ocean.

Rough estimates of the terms are summarized in Table 3. The utility of ^{13}C as a discriminator between biospheric and oceanic exchanges stems from the larger fractionation during terrestrial photosynthesis than during air-to-sea transfer of carbon: the term Δ multiplying the net biospheric sink, N_b, is ~10 times larger than the term ϵ_{ao} multiplying the missing oceanic sink, N_o, in equation (21). However, the use of equation (21) to constrain the carbon budget requires that the isotopic disequilibria associated with the gross fluxes are known as well. For a given $\mathcal{D}_o \times G_o$, the product $\mathcal{D}_b \times G_b$ associated with gross biospheric fluxes is comparable in magnitude to the product $\Delta \times N_b$ associated with net biospheric fluxes (Table 3). Assuming that the oceanic $\mathcal{D}_o$ can be determined by direct measurements [*Quay et al.*, 1992], an underestimate of 0.1‰ in $\mathcal{D}_b$ would translate into an overestimate of 0.3 Gt C yr^{-1} in N_b if Δ = 18‰ and an N_b overestimate of 0.5 Gt C yr^{-1} if Δ = 12‰.

The sensitivity of N_b, the net terrestrial carbon flux, to Δ and $\mathcal{D}_b$ can be investigated using the global budget (equation 21). As has been pointed out by *Lloyd and Farquharson* [1994], Δ multiplies the net flux, while $\mathcal{D}_b$ multiplies the globally averaged gross flux. Thus the appropriate Δ is that associated with the sought-after vegetation types involved in the net carbon uptake and can therefore range between ~4 and ~27‰. We also note that δ_{DEF}-δ_A associated with land use modification is not likely to equal Δ associated with the net biospheric uptake, as different vegetation groups may

Table 3. Typical Values of the Terms in Equation (22) for the 1980s

Description	Parameters	*Schimel et al.* [1996], *Tans et al.* [1993], Gt ‰ yr^{-1}	*Francey et al.* [1995], Gt ‰ yr^{-1}
Atmospheric change	$C_a \frac{\delta}{\delta t}\delta_A$	750 × [-0.02] = -15.0	-22.2
Fossil fuels	$S_{FF} \times (\delta_{FF} - \delta_A)$	5.5 × [-27.2 -(-7.8)] = -149.2	-152.5
Deforestation	$+ S_{DEF} \times (\delta_b - \delta_A)$	1.6 × [-25 -(-7.8)] = -27.52	
Biosphere, gross	$+ G_b \times \mathcal{D}_b^*$	60 × 0.2* = 12	26.5
Biosphere, net	$- N_b \times \Delta^*$	-(-1.8) × 18* = 25.8	
Oceans, gross	$+ G_o \times \mathcal{D}_o$	90 × [0.43] = 38.7	43.8
Oceans, net	$N_o \times \varepsilon_{ao}$	(-2.0) × [-2] = 4.0	

In the third column, values for ^{12}C parameters are taken from *Schimel et al.* [1996] and are representative of 1980-1989 when the atmospheric increase averaged 3.3 Gt C yr^{-1}. The ^{13}C parameters are from *Tans et al.* [1993]. Because the parameters are taken from different sources, the first term does not equal the sum of the remaining terms in this example. Values used by *Francey et al.* [1995] are in the fourth column.

*This study focuses on a reevaluation of Δ and $\mathcal{D}_b$.

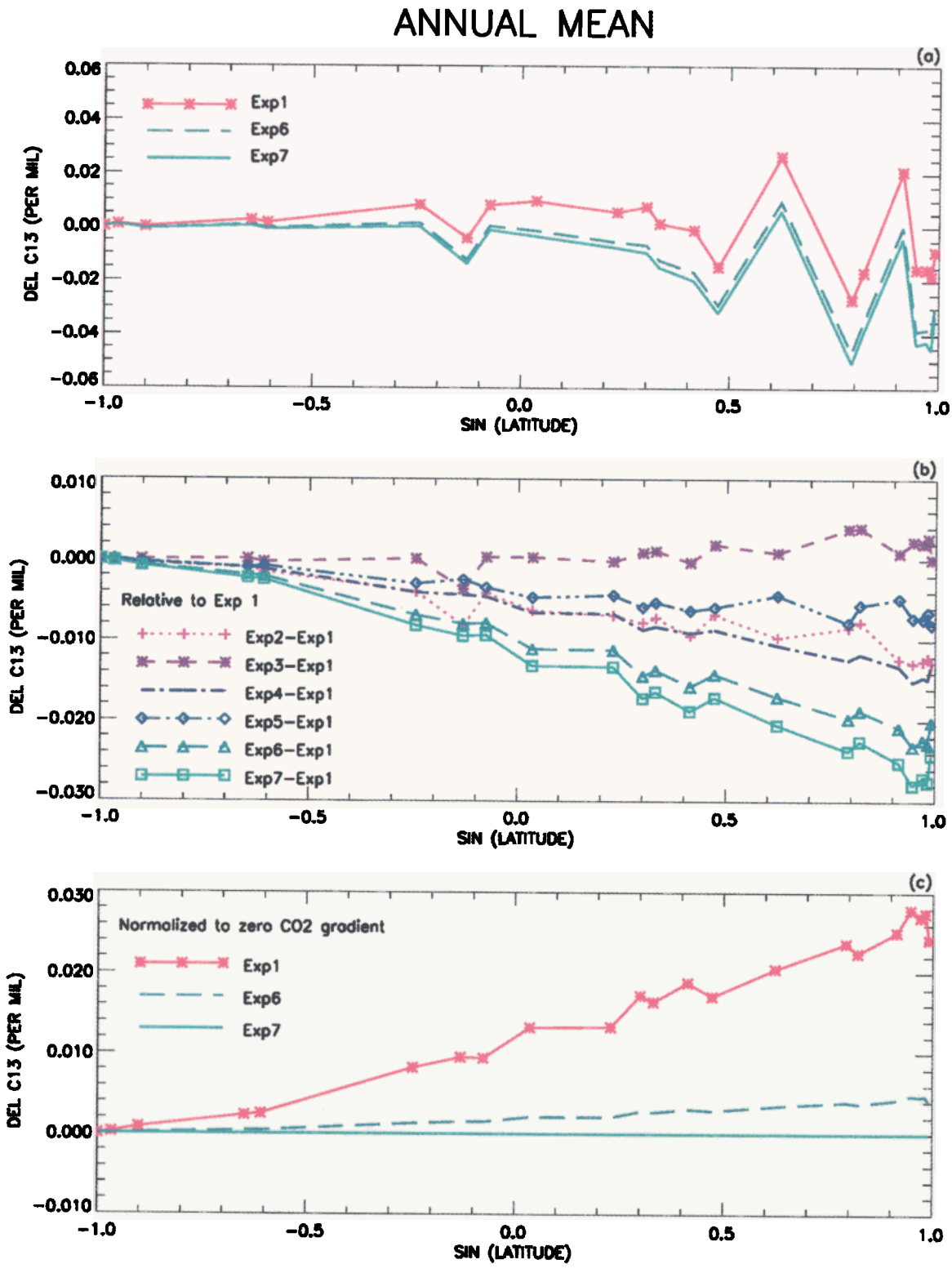

Plate 5. The latitudinal profile in the annually averaged $\delta^{13}C$ simulated for the NOAA monitoring sites in the seven experiments as summarized in Table 3. (a) The modeled profiles for experiments 1,6, and 7, which employ the full variations in Δ and $\mathcal{D}_b$. (b) The departure of the modeled $\delta^{13}C$ profiles in experiments 2–6 from that in experiment 1. (c) Like Plate 5a but normalized to a background CO_2 gradient of zero.

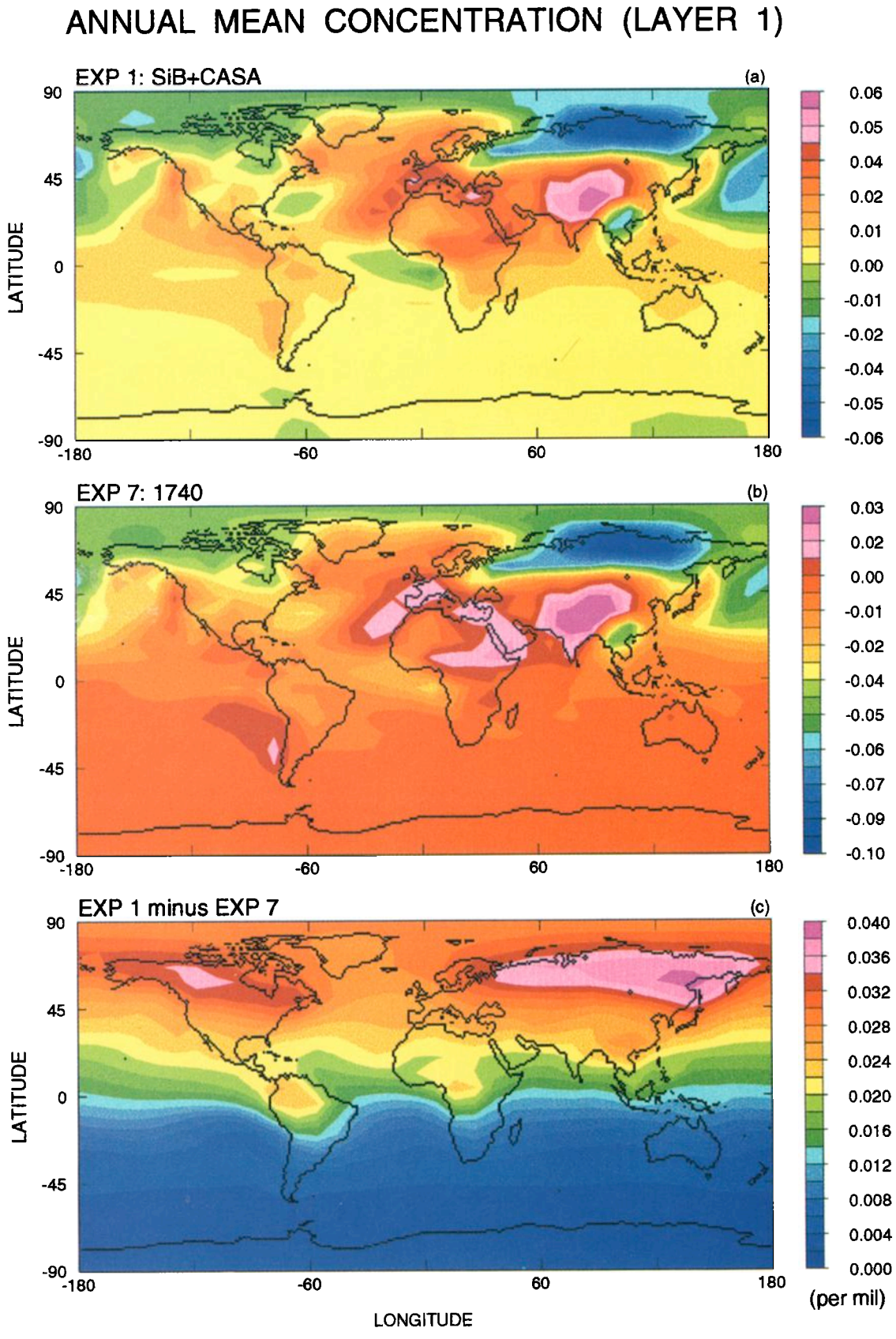

Plate 6. Global distribution of the annually averaged $\delta^{13}C$ for (a) experiment 1, (b) experiment 7 (due to annual mean CO_2 concentrations alone), and (c) experiment 1 minus experiment 7 (due to $\mathcal{D}_b$ alone).

be involved. It is thus inappropriate to combine S_{DEF} and N_b into a single unknown, as is commonly done.

Suppose the values for all variables except for δ_{FF}, N_b, N_o, Δ, $\mathcal{D}_b$ and $\mathcal{D}_o$ are specified as in Table 3. We have assumed a fossil fuel source of 5.5 Gt C yr^{-1}, with an updated $\delta_{FF} = -28.2‰$ [*Andres et al.*, 1996] and a deforestation source of 1.6 Gt C yr^{-1}, with $\delta_{DEF} = -25‰$, typical of tropical rainforests (Table 1b). For the period 1980–1989, the CO_2 growth was ~ 3.3 Gt C yr^{-1}, and the average sink for anthropogenic (fossil fuel plus land use) CO_2 was $N_b + N_o = -3.8$ Gt C yr^{-1} [*Schimel et al.*, 1996]. We can express the biospheric fraction of the sink $r_b = N_b/(N_b + N_o)$ in terms of Δ and $\mathcal{D}_b$ (Figure 10). For a given degree of isotopic disequilibrium between the oceanic fluxes ($\mathcal{D}_o$), the value of r_b decreases, or the ocean sink increases, with increasing Δ and increasing $\mathcal{D}_b$.

The terrestrial portion of the anthropogenic sink dominates for "reasonable" values of Δ, $\mathcal{D}_b$ and $\mathcal{D}_o$. Using Δ = 18‰ and $\mathcal{D}_b$ = 0.2‰ *Tans et al.* [1993] argued that the oceanic isotopic disequilibrium $\mathcal{D}_o$ = 0.43‰ they estimated from the shipboard measurements analyzed by *Quay et al.* [1992] is unlikely, since the oceanic sink would be <0.5 Gt C yr^{-1}(Figure 10a). With the larger value of $\mathcal{D}_b$ obtained here, the oceanic sink may be ~20% of the total sink or ~ 0.7 Gt C yr^{-1} if only C_3 vegetation were involved in the uptake. If net biospheric uptake occurs globally or is confined to C_4 vegetation and $\mathcal{D}_o$= 0.43‰, then the relative biospheric sink would (unrealistically) exceed 100%.

Francey et al. [1995] used a value of $\mathcal{D}_b$ equivalent to 0.44‰and $\mathcal{D}_o$ equivalent to 0.48‰for the same gross fluxes as in Table 3. For a consistent carbon budget scenario, *Heimann and Maier-Reimer* [1996] have deduced a $G_b\mathcal{D}_b$ of 23.4 Gt C ‰yr^{-1}and a $\mathcal{D}_o$ of 0.53‰. The $G_b\mathcal{D}_b$ value translates into a $\mathcal{D}_b$ of 0.39‰for G_b = 60 Gt C yr^{-1}. The values for their parameters also favor a higher oceanic uptake than *Tans et al.* [1993] do. In any case, the oceanic sink remains less than or comparable with the biospheric uptake of anthropogenic (fossil fuel plus deforestation) CO_2.

A high value of $\mathcal{D}_o$ reported is 0.63‰ [*Inoue and Sugimura*, 1985; *Tans et al.*, 1993]. Figure 10c shows the range of r_b as a function of $\mathcal{D}_b$ and Δ for this value of $\mathcal{D}_o$. If biospheric uptake is proportional to the global NPP distribution (Δ ~15‰), a biospheric sink fraction >80% results. The maximum oceanic sink fraction would be ~50%, if the biospheric uptake is by C_3 vegetation only.

The magnitude of the biospheric and oceanic sinks cannot be determined without information about the C_3:C_4 proportions involved in the biospheric uptake and information about $\mathcal{D}_b$. It is very unlikely, however, that the oceanic fraction of the anthropogenic sink could exceed 50%.

In using the north-south gradient to infer the location and magnitudes of the terrestrial sink, our study underlines the importance of the background biosphere, whose gross fluxes contribute non zero background ^{12}C and ^{13}C gradients in the atmosphere. The background gradients need to be subtracted from the total observed atmospheric gradient before

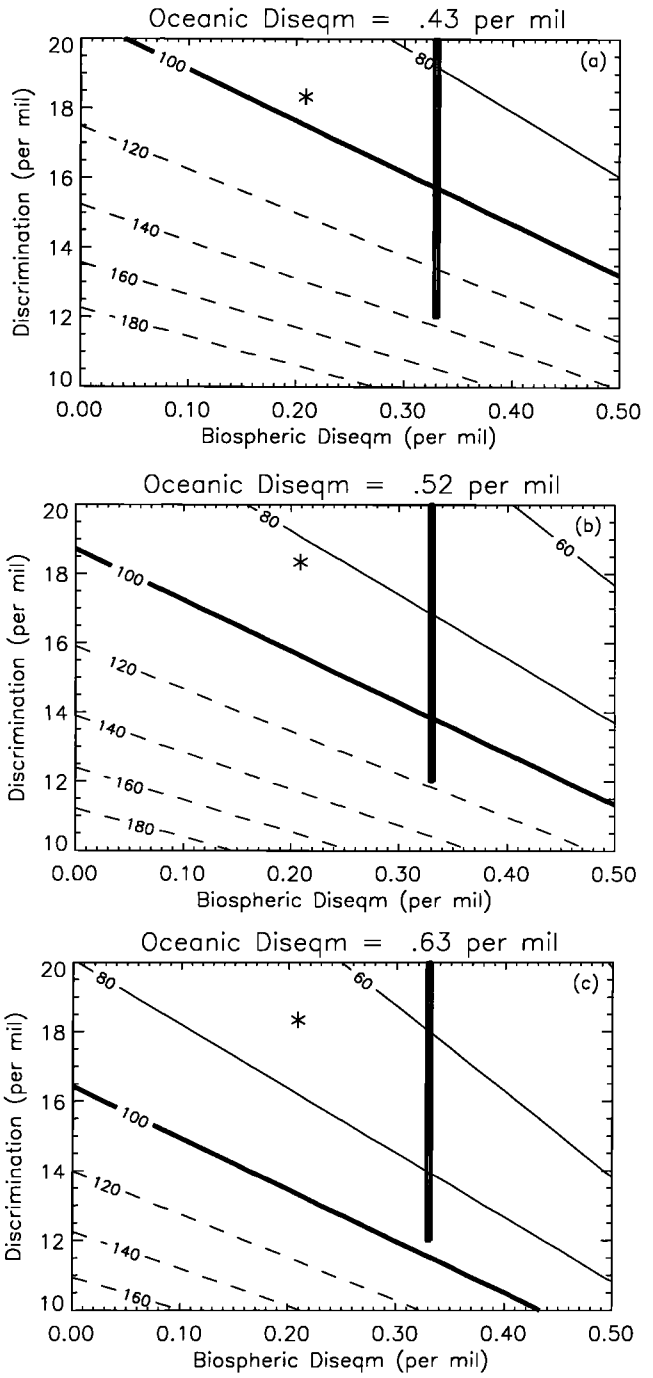

Figure 10. The net biospheric sink, expressed as a fraction of the total anthropogenic CO_2 sink, on the isotopic disequilibrium and photosynthetic discrimination Δ for oceanic isotopic disequilibrium $\mathcal{D}_o$= (a) 0.43‰ (b) 0.52‰ and (c) 0.63‰. The asterisk represents values employed by *Tans et al.* [1993]. The wide bar represents the range estimated in this study.

we can consider contributions by the net sinks. The positive background CO_2 gradient (higher in the northern than in the southern hemisphere) demands a larger combined biospheric and oceanic sink in the northern hemisphere to match the observed CO_2 gradient (compare Figure 1). Furthermore, the

positive CO_2 gradient is accompanied by a negative δ_a gradient, once again demanding a larger net sink than the situation with no gradient from the background biosphere. From the $\delta^{13}C$ perspective, the net sink is primarily biospheric since net oceanic exchange has an atmospheric signature that is 10 times less than net biospheric exchange. In other words, the combined CO_2 and δ_a gradients due to the background biosphere favor a predominantly terrestrial sink.

An analysis of the carbon budget for 1991–1994 has been carried out by *Keeling et al.* [1996] using the variations in atmospheric oxygen. Compared to 1980–1989, this period has a stronger fossil fuel source, ~5.8 Gt C yr^{-1}, slower growth of atmospheric CO_2, ~ 2.1 Gt C yr^{-1}, and a slowdown in $\delta^{13}C$ decrease rate to $\sim -0.01‰ yr^{-1}$ [*Francey et al.*, 1995]. *Keeling et al.* [1996] found that the land and oceans removed 2.0±0.9 and ~1.7±0.9 Gt C yr^{-1}, respectively, of the fossil fuel CO_2. Adding the deforestation flux of 1.6 Gt C yr^{-1} to their land sink increases their terrestrial uptake to −3.6 Gt C yr^{-1}. This would yield a biospheric uptake fraction $r_b = 3.6/(3.6 + 1.7) = 68\%$. There is no unique way to match their oxygen-based budget with a ^{13}C-based budget without additional information. For example, an $r_b = 68\%$ can be obtained by the combination $\mathcal{D}_o = 0.63‰$ and $\Delta = 18‰$ or the combination $\mathcal{D}_o = 0.52‰$ and $\Delta = 20‰$. About ~85% in the former and 100% in the latter example of terrestrial uptake would be in C_3 regions. A large background $\mathcal{D}_b$ and/or $\mathcal{D}_o$ leaves a large atmospheric signature and needs to be accompanied by C_4 uptake with less photosynthetic discrimination than C_3 uptake. It is premature to estimate the geographic distribution of the net biospheric sinks without a parallel treatment of the geographically varying δ_a signal due to gross oceanic fluxes.

8. Implication for Measurement Strategy and Data Acquisition

In this paper, we combined detailed models of the ^{13}C:^{12}C fractionation associated with photosynthesis and respiration to investigate the geographic and temporal variations of ^{13}C in the terrestrial biosphere and the atmosphere. Our findings from the atmospheric transport experiments are summarized in Table 4. Because of the long memory of soil carbon, unravelling the information contained in present-day atmospheric $\delta^{13}C$ variations requires understanding of the dynamics of the biosphere on decadal to centennial time scales.

The simulated ^{13}C distributions and the application to the contemporary carbon budget are sensitive to the many assumptions necessitated by the lack of detailed atmospheric and biospheric observations that could constrain the calculations. In the following, we suggest measurements that can help cross-check the results and/or improve the treatment of important processes in the models.

1. Inferences about the location and magnitude of the anthropogenic carbon sinks rely on geographic and temporal variations of atmospheric CO_2 and $\delta^{13}C$ in the planetary boundary layer. Resolution of the magnitude of the rectifier effect is thus a prerequisite to using the latitudinal information. This can be addressed with vertical profiles of CO_2 and $\delta^{13}C$ in the continental planetary boundary layer [*Bakwin et al.*, 1995] in conjunction with flux measurements [*Wofsy et al.*, 1993].

2. The present-day value of Δ necessary for deconvolving the global carbon budget is determined by the relative contributions of C_3 and C_4 plants to the biospheric uptake. Concentrating the biospheric sink in C_3 areas would favor a larger uptake by the oceans. This finding argues for CO_2 fertilization and other direct biospheric manipulation experiments across vegetation gradients that include both C_3 and C_4 types.

3. Our lack of quantitative estimate of photosynthetic discrimination worldwide is reflected in the large range in flux-weighted annual-mean $\overline{\overline{\Delta}}$. We show that, where CO_2 fluxes are seasonal, $\overline{\overline{\Delta}}$ may be different by several per mils from the annual-mean Δ without flux weighting and from a one-time measurement of Δ. A 3‰ overestimate of $\overline{\overline{\Delta}}$ can translate into 0.7 Gt C yr^{-1} or 20% underestimate in the magnitude of the biospheric sink. Here we have employed the SiB2-GCM Δ, whose formulation is rooted in extensive theoretical and field studies, but whose magnitudes are dependent on the simulated GCM climate. The use of a different climatology or a different set of fluxes in the weighting may yield a different value of $\overline{\overline{\Delta}}$. This argues for the simultaneous measurements of $F_{ap}(t_s, t)$ and $\Delta(t_s, t)$, such as the eddy-flux correlation measurements of *Lloyd et al.* [1996] and *Krujit et al.* [1996]. Since long time series are critical, we suggest extending the measurements of *Lloyd et al.*

Table 4. Summary of Biospheric Fractionation Factors Important for Explaining Different Aspects of the Atmospheric $\delta^{13}C$ Variation

Atmospheric Signal	Important Biospheric Fractionation Factors
δ_A seasonal cycle at individual sites	Δ seasonality, $\mathcal{D}_b$
Trend in δ_A amplitudes	trend in $\mathcal{D}_b$
Latitudinal profiles in annual mean δ_A	latitudinal profile of $\mathcal{D}_b$
Trend in annual mean δ_A (y)	trend in C_3:C_4 composition
Global carbon budget	flux-weighted annual mean Δ of vegetation associated with net sink;
	flux-weighted global annual mean $\mathcal{D}_b$

[1996] and *Krujit et al.* in time and those of *Wofsy et al.* [1993] to include $\delta^{13}C$.

4. A major determining parameter for the carbon budget is the annual-mean flux-weighted $\widetilde{\mathcal{D}_b}$. A long-term measurement program is needed to establish temporal variations of δ_b, the isotopic composition of the respired CO_2. *Lloyd et al.* [1996] have pointed out the different methods available. The most promising method appears to "predict" $\delta^{13}C$ based on CO_2 concentrations in the boundary layer using empirical relationships between CO_2 and $\delta^{13}C$. As we have shown, there may be variations in $\delta^{13}C$ without variations in CO_2 fluxes, because the relative contributions from the different pools vary through the year. Hence the relationships between CO_2 and $\delta^{13}C$ in the boundary layer need to be established through all seasons and for all major ecosystems. *Miranda et al.* [1997] show that such relationships, when combined with measurements of foliar $\delta^{13}C$, can be used to monitor seasonal variations in C_3:C_4 composition in a cerrado. Snap shot measurements of δ_b, such as those made in intensive field campaigns, provide the inter-pool variations δ_k^*, which we show to cancel out to first order when summed over all the pools. Measurements and analysis of the ^{14}C:^{12}C ratio in different soil pools [e.g., *Trumbore*, 1993] do not provide information about the fluxes from the different soil pools. However, they constrain the modeled mass distributions of soil carbon and their turnover times.

5. The respired δ_b integrated over all the biospheric pools is dependent on f_k, the fraction of the respired flux from each pool. Our study shows the importance of the microbial and woody pools. It is very difficult to separate the contributions from the different pools in the total CO_2 measurement. However, the small seasonal variations in the respired $\delta^{13}C$ will provide a cross-check, albeit not a very stringent one, on the product $f_k\ \delta_{b,k}$. Also, measurements of seasonal variations in the ^{14}C:^{12}C ratio of the respired CO_2 will provide additional constraints on f_k. A factor ignored in the calculations in this study is root respiration, which may be constrained by simultaneous measurements of the fluxes of ^{12}C, ^{13}C and ^{14}C from the soils [*Trumbore et al.*, 1995].

6. We have assumed that the functioning of the biosphere has not changed with a 25% increase in atmospheric CO_2 since the preindustrial era. In particular, we have assumed that $\Delta(x, y, t_s, t)$, $f_k(x, y, t_s, t)$, and therefore allocation have remained the same in the past 200 years. The value Δ, in principle, should change with changes in climate and carbon assimilation. Recent field and laboratory measurements have shown, for example, that root-shoot ratios change in response to CO_2 fertilization. Whether these changes are significant enough to impact the contemporary carbon budget remains to be investigated.

Notation

Independent Variables and Operators

x, y east-west, north-south coordinate.

t_s time, seasonal (<1 year) variations.

t time, longer term (>1 year) varations.

$\widetilde{(\ldots)}$ flux-weighted annual mean (integration over t_s).

$\overline{(\ldots)}$ flux-weighted long-term mean (integration over t).

Subscripts

A atmosphere, total response.

a atmosphere, response to an individual forcing.

b biosphere involved in heterotrophic respiration.

DEF deforestation and land use modification.

FF fossil fuels.

o ocean.

Variables

A_n gross CO_2 assimilation rate.

$\mathcal{A}$ seasonal amplitude of $\delta^{13}C$ in the atmosphere.

C_A total distribution of carbon in the atmosphere, equal to 715 Gt C globally.

C_a atmospheric carbon distribution in response to a source/sink.

F_{ij} ^{12}C fluxes from pool i to pool j. Positive into the atmosphere.

f_k fraction of respired CO_2 from biospheric pool k.

g_s stomatal resistance.

G_b gross CO_2 exchanges between the atmosphere and biosphere, equal to F_{ba}.

G_o gross CO_2 exchanges between the atmosphere and ocean.

h_s relative humidity of the ambient air.

N_b net fluxes of CO_2 exchange between the atmosphere and biosphere, equal to $F_{ap} + F_{ba}$.

N_o net fluxes of CO_2 exchange between the atmosphere and ocean. $N_b + N_o$ = total sink for anthropogenic CO_2.

p_i, p_s, p_a intercellular, leaf surface and ambient CO_2 partial pressures, respectively.

P total atmospheric pressure.

r_b biospheric fraction of total anthropogenic sink, equal to $N_b/(N_b + N_o)$.

S_{FF} strength of CO_2 emission from fossil fuel combustion, equals 5.5 Gt C yr^{-1}.

S_{DEF} strength of CO_2 emission from land-use modification, equals 1.6 Gt C yr^{-1}.

δ_A $\delta^{13}C$ of atmospheric CO_2, equal to $-7.8‰$ in 1988.

δ_a atmospheric $\delta^{13}C$ response to exchanges with a single reservoir.

δ_b $\delta^{13}C$ of the respired CO_2.

$\delta_{b,k}$ $\delta^{13}C$ of biospheric pool k.

$\delta_k{}'$ departure of $\delta_k(t)$ from the preindustrial steady state value for pool k.

$\overline{\widetilde{\delta_k^*}}$ departure of the preindustrial steady state $\overline{\widetilde{\delta_k}}$ for pool k from the all-pool flux-weighted mean $\overline{\widetilde{\delta_b}}$.

Δ photosynthetic discrimination, 4–27 ‰ .

$\mathcal{D}_b$ isotopic disequilibrium between gross photosynthetic and respiratory fluxes of carbon.

$\mathcal{D}_o$ isotopic disequilibrium between gross fluxes of CO_2 into and out of the ocean.

τ_k age of biospheric pool k.

ϵ_{ao} fractionation coefficient for air-to-sea flux of CO_2.

Acknowledgments. We thank Chris Potter for providing output from the 1992 version of CASA. Principal support for this work is provided by the NASA Office of the Mission to Planet Earth to the Sellers-Mooney EOS-IDS team. Other support includes the NSF/DOE/NASA/USDA TECO Program and Canadian Atmospheric Environment Service grants to I.Y.F. and a grant from the DOE NIGEC/WESTGEC program to C.B.F. and J.A.B. C.M.M. was supported by DOE Fellowship for Global Change Research, and J.T.R. was supported by a NASA Global Change Fellowship. Very helpful comments on the manuscript by Pieter Tans and two anonymous reviewers and discussions with Ian Enting are gratefully acknowledged. We also thank Stephanie Meyn for her help in preparing the final manuscript.

References

Andres, R. J., G. Marland, T. Boden, and S. Bischof, Carbon dioxide emissions from fossil fuel consumption and cement manufacture, 1751–1991; and an estimate of their isotopic composition and latitudinal distribution, in *1993 Global Change Institute,* edited by T. Wigley and D. Schimel, Cambridge Univ. Press, New York, 1996.

Bakwin, P. S., P.P. Tans, and E. Quesnell, Measurement of carbon dioxide on a very tall tower, *Tellus, Ser. B, 47,* 535, 1995.

Ball, J. T., I.E. Woodrow, and J.A. Berry, A model predicting stomatal conductance and its contribution to the control of photosynthesis under different environmental conditions, *Progress in Photosynthesis Research,* vol. 4, edited by J. Biggins, pp. 221–224, Martinus-Nijhoff, Zoetermeer, Netherlands, 1987.

Bolin, B., and H. Rodhe, A note on the concepts of age distribution and transit time in natural reservoirs, *Tellus, 25,* 58–62, 1973.

Broadmeadow, M.S.J., and H. Griffiths, Carbon isotope discrimination and the coupling of CO_2 fluxes with forest canopies, in *Stable Isotopes and Plant Carbon-Water Relations,* edited by J.R. Ehleringer, A.E. Hall, and G.D. Farquhar, chap. 8, pp. 109–130, Academic, San Diego, Calif., 1993.

Ciais, P., P.P. Tans, M. Trolier, J.W.C. White, and R.J. Francey, A large northern hemisphere terrestrial CO_2 sink indicated by $^{13}C/^{12}C$ of atmospheric CO_2, *Science, 269,* 1098–1100, 1995a.

Ciais, P., P.P. Tans, J.W.C. White, M. Trolier, R.J. Francey, J.A. Berry, D.R. Randall, P.J. Sellers, J.G. Collatz, and D.S. Schimel, Partitioning of ocean and land uptake of CO_2 as inferred by $\delta^{13}C$ measurements from the NOAA/CMDL global air sampling network, *J. Geophys. Res., 100,* 5050–5070, 1995b.

Collatz, G.J., J.T. Ball, C. Grivet, and J.A. Berry, Physiological and environmental regulation of stomatal conductance, photosynthesis, and transpiration: A model that includes a laminar boundary layer, *Agric. For. Meteorol., 54,* 107–136, 1991.

Collatz, G.J., M. Ribas-Carbo, and J.A. Berry, Coupled photosynthesis - stomatal conductance model for leaves of C_4 plants, *Aust. J. Plant Physiol., 19,* 519–538, 1992.

Denning, A.S., I. Fung, and D. Randall, Strong simulated meridional gradient of atmospheric CO_2 due to seasonal exchange with the terrestrial biota, *Nature, 376,* 240–242, 1995.

Dorman, J.L., and P.J. Sellers, A global climatology of albedo, roughness length and stomatal resistance for atmospheric general circulation models as represented by the simple biosphere model (SiB), *J. Appl. Meteorol., 28,* 833–855, 1989.

Emanual, W.R., G.H.G. Killough, and J.S. Olsen, Modelling the circulation of carbon in the world's terrestrial ecosystem, in *Carbon Cycle Modelling,* edited by B. Bolin, pp. 335–364, John Wiley, New York, 1981.

Enting, I.G., C.M. Trudinger, R.J. Francey, and H. Granek, Synthesis inversion of atmospheric CO_2 using GISS tracer transport model, *Tech. Rep. 29,* Div. of Atmos. Sci., Commonw. Sci. and Ind. Res. Organ., Mordialloc, Victoria, Australia, 1993.

Enting, I.G., C.M. Trudinger, and R.J. Francey, A synthesis inversion of the concentration and $\delta^{13}C$ of atmospheric CO_2, *Tellus, Ser. B, 47,* 35–52, 1995.

Evans, J.R., T.D. Sharkey, J.A. Berry, and G.D. Farquhar, Carbon isotope discrimination measured concurrently with gas exchange to investigate CO_2 diffusion in leaves of higher plants, *Aust. J. Plant Physiol., 13,* 281–293, 1986.

Farquhar, G.D., S. von Caemmerer, and J.A. Berry, A biochemical model of photosynthetic CO_2 in leaves of C_3 species, *Planta, 149,* 78–90, 1980.

Farquhar, G.D., M.H. O'Leary, and J.A. Berry, On the relationship between carbon isotope discrimination and the intercellular carbon dioxide concentration in leaves, *Aust. J. Plant Physiol., 9,* 121–137, 1982.

Farquhar, G.D., J.R. Ehleringer, and J.A. Berry, Carbon isotope discrimination and photosynthesis, *Annu. Rev. Plant Physiol. Plant Mol. Biol., 40,* 503–537, 1989.

Flanagan, L.B., J.R. Brooks, G.T. Varney, S.C. Berry, and J.R. Ehleringer, Carbon isotope discrimination during photosynthesis and the isotope ratio of respired CO_2 in boreal forest ecosystems, *Global Biogeochem. Cycles, 10,* 629–640, 1996.

Francey, R.J., and G.D. Farquhar, An explanation of $^{13}C/^{12}C$ variations in tree rings, *Nature, 297,* 28–31, 1982.

Francey, R.J., P.P. Tans, C.E. Allison, I.G. Enting, J.W.C. White, and M. Trolier, Changes in oceanic and terrestrial carbon uptake since 1982, *Nature, 324,* 237–238, 1986.

Friedli, H., H. Lotscher, H. Oeschger, U. Siegenthaler, and B. Stauffer, Ice core record of the $^{13}C/^{12}C$ ratio of atmospheric CO_2 in the past two centuries, *Nature, 324,* 237–238, 1986.

Fung, I., Models of oceanic and terrestrial sinks of anthropogenic CO_2: A review of the contemporary carbon cycle, in *Biogeochemistry of Global Change: Radiatively Active Trace Gases,* edited by R. Oremland, pp. 166–189, Chapman and Hall, New York, 1993.

Fung, I., K. Prentice, E. Matthews, J. Lerner, and G. Russell, A 3-D tracer model study of atmospheric carbon dioxide: Response to seasonal exchanges with the terrestrial biosphere, *J. Geophys. Res., 88,* 1282–1294, 1983.

Fung, I., C.J. Tucker, and K.C. Prentice, Application of advanced very high resolution radiometer vegetation index to study atmosphere - biosphere exchange of CO_2, *J. Geophys Res., 92,* 2999–3015, 1987.

Fung, I., J. John, J. Lerner, E. Matthews, M. Prather, L.P. Steele, and P.J. Fraser, Three-dimensional model synthesis of the global methane cycle, *J. Geophys. Res., 96,* 13033–13065, 1991.

Hansen, J., G. Russell, D. Rind, P. Stone, A. Lacis, S. Lebedeff, R. Ruedy, and L. Travis, Efficient three-dimensional global models for climate studies: Models I and II, *Mon. Weather Rev., 111,* 609–662, 1983.

Heimann, M., and C.D. Keeling, A three-dimensional model of atmospheric CO_2 transport based on observed winds, 2, Model description and simulated tracer experiments, in *Aspects of Climate Variability in the Pacific and the Western Americas, Geophys. Monogr. Ser.,* vol. 55, edited by D.H. Peterson, pp. 237–275, AGU, Wahsington, D.C., 1989.

Heimann, M., and E. Maier-Reimer, On the relations between the oceanic uptake of CO_2 and its carbon isotopes, *Global Biogeochem. Cycles, 10,* 89–110, 1996.

Inoue, H., and Y. Sugimura, Carbon isotopic fractionation during the exchange process between air and sea water under equilibrium and kinetic conditions, *Geochem. Cosmochim., Acta, 49,* 2453–2460, 1985.

Keeling, C.D., The concentrations and isotopic abundances of atmospheric carbon dioxide in rural areas, *Geochim. Cosmochim. Acta, 13,* 332–334, 1958.

Keeling, C.D., The concentration and isotopic abundances of atmospheric carbon dioxide in rural and marine air, *Geochim Cosmochim Acta, 13,* 277–298, 1961.

Keeling, C.D., S.C. Piper, and M. Heimann, A three - dimensional model of atmospheric CO_2 transport based on observed winds, 4, Mean annual gradients and interannual variations, in *Aspects of Climate Variability in the Pacific and the Western Americas, Geophys. Monogr. Ser.,* vol. 55, edited by D.H. Peterson, pp. 305–363, AGU, Washington, D.C., 1989a.

Keeling, C.D., R.B. Bacastow, A.F. Carter, S.C. Piper, T.P. Whorf, M. Heimann, W.G. Mook, and H. Roeloffzen, A three-dimensional model of atmospheric CO_2 transport based on observed winds, 1, Analysis of observational data, in *Aspects of Climate Variability in the Pacific and the Western Americas, Geophys. Monogr. Ser.,* vol. 55, edited by D.H. Peterson, pp. 165–236, AGU, Washington, D.C., 1989b.

Keeling, C.D., T.P. Whorf, M. Wahlen, and J. van der Plicht, Interannual extremes in the rate of rise of atmospheric carbon dioxide since 1980, *Nature, 375,* 666–670, 1995.

Keeling, C.D., J.F.S. Chin, and T.P. Whorf, Increased activity of northern vegetation inferred from atmospheric CO_2 measurements, *Nature, 382,* 146–149, 1996.

Körner, C., G.D. Farquhar, and S.C. Wong, Carbon isotope discrimination by plants follows latitudinal and altitudinal trends, *Oecologia, 88,* 30–40, 1991.

Krujit, B., J. Lloyd, J. Grace, J.A. McIntyre, D.D. Farquhar, A.C. Miranda, and P. McCracken, Sources and sinks of CO_2 in Rondonia tropical rainforest, in *Amazonian Deforestation and Climate,* edited by J.H.C. Gash, C.A. Nobre, J.M. Roberts, and R.L. Victoria, chap. 19, pp. 331–351, John Wiley, New York, 1996.

Lauteri, M., E. Brugnoli, and L. Spaccino, Carbon isotope discrimination in leaf soluble sugars and in whole-plant dry matter in *helianthus annus l.* grown under different water conditions, in *Stable Isotopes and Plant Carbon-Water Relations,* edited by J.R. Ehleringer, A.E. Hall, and G.D. Farquhar, chap. 7, pp. 93–108, Academic, San Diego, Calif., 1993.

Leuenberger, M., U. Siegenthaler, and C.C. Langway, Carbon isotope composition of atmospheric CO_2 during the last ice age from an Antarctic ice core, *Nature, 357,* 488–490, 1992.

Lloyd, J., and G.D. Farquhar, ^{13}C discrimination during CO_2 assimilation by the terrestrial biosphere, *Oecologia, 99,* 201–215, 1994.

Lloyd, J., et al., Vegetation effects on the isotopic composition of atmospheric CO_2 at local and regional scales: Theoretical aspects and a comparison between rain forest in Amazonia and a boreal forest in Siberia, *Aust. J. Plant Physiol., 23,* 371–399, 1996.

Lüdeke, M.K.B., et al., The Frankfurt Biosphere Model: A global process oriented model for the seasonal and longterm CO_2 exchange between terrestrial ecosystems and the atmosphere, *Clim. Res., 4,* 143–166, 1994.

Miranda, A.C., J.S. Miranda, J. Lloyd, J. Grace, R.J. Francey, J.A. McIntyre, P. Meir, P. Riggan, R. Lockwood, and J. Brass, Fluxes of carbon, water and energy over Brazilian cerrado: An analysis using eddy covariance and stable isotopes, *Plant, Cell Environ., 20,*, 315, 1997.

Nakazawa, T., S. Morimoto, S. Aoki, and M. Tanaka, Time and space variations of carbon isotopic ratio of tropospheric carbon dioxide over Japan, *Tellus, Ser. B., 45,* 209–215, 1993.

O'Leary, M.H., Carbon isotope fraction in plants, *Phytochemistry, 20,* 553–567, 1981.

O'Leary, M.H., Multiple isotope effects on enzyme-catalyzed reactions, *Annu. Rev. Biochem., 58,* 337–401, 1989.

Potter, C.S., J.T. Randerson, C.B., Field, P.A. Matson, P.M. Vitousek, H.A. Mooney, and S.A. Klooster, Terrestrial ecosystem production: A process model based on global satellite and surface data, *Global Biogeochem. Cycles, 7,* 811–841, 1993.

Quay, P.D., B. Tilbrook, and C.S. Wong, Oceanic uptake of fossil fuel CO_2: Carbon-13 evidence, *Science, 256,* 74–79, 1992.

Randall, D.A., D.A. Dazlich, C. Zhang, J.A. Collatz, A.S. Denning, S.O. Los, C.B. Field, I. Fung, C.O. Justice, and C.J. Tucker, A revised land-surface parameterization (SiB2) for atmospheric GCMs, 3, The greening of the Colorado State University general circulation model, *J. Clim., 9,* 738–763, 1996.

Randerson, J.T., M.V. Thompson, C.M., Malmstrom, C.B. Field, and I.Y. Fung, Substrate limitations for heterotrophs: Implications for models that estimate the seasonal cycles of atmospheric CO_2, *Global Biogeochem. Cycles, 10,* 585–602, 1996.

Rodhe, H., Modeling biogeochemical cycles, in *Global Biogeochemical Cycles,* edited by S.S. Butcher, R.J. Charlson, G.H. Orians, and G.V. Wolfe, chap. 4, pp. 55–72, Academic, San Diego, Calif., 1992.

Russell, G.L., and J.A. Lerner, A new finite-differencing scheme for the tracer transport equation, *J. Appl. Meteorol., 20,* 1483–1498, 1981.

Schimel, D., et al., Radiative forcing of climate change, in *Climate Change, 1995: The Science of Climate Change,* edited by J.T. Houghton, L.G. Meira Filho, B.A. Callandar, N. Harris, A. Kattenberg, and K. Maskell, chap. 2, pp. 65–131, Cambridge Univ. Press, New York, 1996.

Schimel, D.S., B.H. Braswell, E.A. Holland, R. McKeown, D.S. Ojima, T.H. Painter, W.J. Parton, and A.R. Townsend, Climatic, edaphic, and biotic controls over storage and turnover of carbon in soils, *Global Biogeochem. Cycles, 8,* 279–293, 1994.

Sellers, P.J., D.A. Randall, J.A. Collatz, J. Berry, C. Field, D.A. Dazlich, and C. Zhang, A revised land-surface parameterization (SiB2) for atmospheric GCMs, 1, Model Formulation, *J. Clim., 9,* 676–705, 1996a.

Sellers, P.J., S.O. Los, C.J. Tucker, C.O. Justice, D.A. Dazlich, G.J. Collatz, and D.A. Randall, A revised land-surface parameterization (SiB2) for atmospheric GCMs, 2, The generation of global fields of terrestrial biophysical parameters from satellite data, *J. Clim., 9,* 706–737, 1996b.

Tans, P.P., On calculating the transfer of carbon-13 in reservoir models of the carbon cycle, *Tellus, Ser. B., 32,* 464–469, 1980.

Tans, P.P., I.Y. Fung, and T. Takahashi, Observational constraints on the global atmospheric CO_2 budget, *Science, 247,* 1431–1438, 1990.

Tans, P.P., J.A. Berry, and R.F. Keeling, Oceanic $^{13}C/^{12}C$ observations: A new window on ocean CO_2 uptake, *Global Biogeochem. Cycles, 7,* 353–368, 1993.

Trolier, M., J.W.C. White, P.P. Tans, K.A. Masarie, and P.A. Gemery, Monitoring the isotopic composition of atmospheric CO_2: Measurements from NOAA global air sampling network, *J. Geophys. Res., 101,* 25897–25916, 1996.

Trumbore, S.E., Comparison of carbon dynamics in tropical and temperate soils using radiocarbon measurements, *Global Biogeochem. Cycles, 7,* 275–290, 1993.

Trumbore, S.E., E.A. Davidson, B. Camargo, D.C. Nepstad, and L.A. Martinelli, Belowground cycling of carbon in forests and pastures of eastern amazonia, *Global Biogeochem. Cycles, 9,* 515–528, 1995.

Wofsy, S.C., M.L. Goulden, J.E. Munger, S.-M. Fan, P.D. Bakwin, B.C. Daube, S.L. Bassow, and F.A. Bazzaz, Net exchange of CO_2 in a mid-latitude forest, *Science, 260,* 1314–1316, 1993.

F. Badeck, Laboratoire d'Ecologie Vegetale, Universite de Paris Sud XI, 91405 Orsay, France (email: Franz.Badeck@eco.u-psud.fr)

J. Berry, C. Field, C. Malmström, J. Randerson, and M. Thompson, Carnegie Institution of Washington, Department of Plant Biology, Stanford, CA 94305. (email: joeberry@biosphere.stanford.edu, chris@jasper.stanford.edu, carolyn@jasper.stanford.edu, orcinus@rosebud.stanford.edu, matt@arbutus.Stanford.edu)

G. J. Collatz, NASA Goddard Space Flight Center, Code 923, Greenbelt, MD 20771. (email: jcollatz@biome.gsfc.nasa.gov)

A. S. Denning and D. Randall, Department of Atmospheric Sciences, Colorado State University, Ft. Collins, CO 80521. (email: denning@esm.ucsb.edu, randall@redfish.atmos.colostate.edu)

I. Fung, School of Earth and Ocean Sciences, University of Victoria. P.O. Box 3055, Canada V8W 3P6. (email: inez@garryoak.seos.uvic.ca)

J. John, Department of Applied Physics, Columbia University, New York, NY 10025. (email: jasmin@garryoak.seos.uvic.ca)

P. J. Sellers, NASA Johnson Space Flight Center, Code CB, Houston, TX 77058. (email: PSellers@ems.jsc.nasa.gov)

P. M. Vitousek, Department of Biological Sciences, Stanford University, Stanford, CA 94305. (email: vitousek@leland.stanford.edu)

(Received September 30, 1996; revised April 10, 1997; accepted June 9, 1997.)